2013-05-29

The Development of a Sensitive Manipulation Platform

Nigel B. Cochran
Worcester Polytechnic Institute

THE DEVELOPMENT OF A SENSITIVE MANIPULATION PLATFORM

By

Nigel Cochran

A Thesis

Submitted to the Faculty

of the

WORCESTER POLYTECHNIC INSTITUTE

in partial fulfillment of the requirements for the

Degree of Master of Science

in

Robotics Engineering

by

_____

May 29, 2013

APPROVED:

_____

Dr. Eduardo Torres-Jara, Advisor

_____

Dr. Cagdas Onal, Thesis Committee Member

_____

Dr. Stephen Nestinger, Thesis Committee Member

Abstract

This thesis presents an extension of sensitive manipulation which transforms tactile sensors away from end effectors and closer to whole body sensory feedback. Sensitive manipulation is a robotics concept which more closely replicates nature by employing tactile sensing to interact with the world. While traditional robotic arms are specifically designed to avoid contact, biological systems actually embrace and intentionally contact the environment. This arm is inspired by these biological systems and therefore has compliant joints and a tactile shell surrounding the two primary links of the arm. The manipulator has also been designed to be capable of both industrial and humanoid style manipulation. There are an untold number of applications for an arm with increased tactile feedback primarily in dynamic environments such as in industrial, humanoid, and prosthetic applications. The arm developed for this thesis is intended to be a desktop research platform, however, one of the most influential applications for increased tactile feedback is in prosthetics which are operate in ever changing and contact ridden environments while continuously interacting with humans. This thesis details the simulation, design, analysis, and evaluation of a the first four degrees of freedom of a robotic arm with particular attention given to the design of modular series elastic actuators in each joint as well as the incorporation of a shell of tactile sensors.

Acknowledgements

Like another experience I had a WPI, working on this project was “one of the best things I never want to do again.” Luckily, I did not have to do all of the work on my own and there were countless people who supported me along the way. First and foremost, I have to thank my advisor, Professor Eduardo Torres-Jara. You gave me not one but two truly unique and challenging projects while I was here that I will forever look back fondly upon. Additionally, if it were not for you and your generosity, I would not have stayed at WPI to do my master’s degree. You’ve made a huge impact on my life and I can’t wait to see what kind of projects you develop with other students in the future.

I would also like to thank my committee members, Professor Cagdas Onal and Professor Stephen Nestinger. The meetings and feedback from both of you were very beneficial and helped to elevate my paper. I would like to add a special thanks to Professor Nestinger for the multiple hours spent helping me on some of the more challenging mathematical problems.

I also have to thank Vadim. You are responsible for all of this. Thank you so much for getting me involved in academic research and then happily answering all of my questions along the way. I would also like to thank you for all of the time you spent going over my design with me and for the few times you gave me a verbal smack on the back of the head and told me what to do when I felt overwhelmed. I hope we get the chance to work together instead of just next to each other someday. Also, here is your tap:

Come get it whenever you want. You can tap the holes though. I have a bad track record.

Ennio, thank you and good luck next year. Thank you for always pushing me to do things the right way and design something innovative instead of safe. Spending the time talking to you as we brainstormed ideas was invaluable and the arm was genuinely better because of you and your ideas. I must also say I am sorry. Vadim and I have now left you two almost mechanically complete robots that you will be making work. You have a real challenge ahead of you but there is no one I know better suited to the work. I hope I get the chance to repay you for all of your help.

To Janine. It's finally over…. until I find a new challenge. Thank you for all of your support. You encourage me to do things before I even realize I want to do them. Thank you for your sheer presence or kind words melting the stress away from me even if I didn't always show my appreciation at the time.

To my family, I am still alive. I know it might have been hard to tell at times. It's surprisingly hard to find time to call when working in a lab with no cell reception or windows. It seemed like I would never stop working before my parents' bed time. Mom, thank you for always pushing me to my limits and finding ways to challenge me academically. Dad, thank you for all of your support and help whenever I needed it regardless of what it was. Hopefully I'll be seeing a little bit more of everyone now.

To Catherine, Michael, Anthony, and Carly, it was a pleasure working with you all. Catherine, I know you'll have the rest of the arm done soon and it will work and look great. Carly, thank you for your help with my papers. Mike and Anthony, it was fun getting to know you guys in the lab.

To everyone that helped me on the different stages of this project thank you. Thank you to Ross and Kirk for your help on the kinematics and dynamics. To Matt, Kevin and Chris, thanks for all of the help in the machine shop. It was nice shaking some of the rust off and getting back into the machine

shop. Hopefully I wasn't too much of an inconvenience. To Paul and Chris thanks for your help with assembling the arm and keeping me company in the lab. To the others that helped me and I forgot to mention by name, I am sorry; it's been a long year.

Tracey, everyone in our lab makes your life so difficult. At least there is one less of us now. Thank you for staying on top of all of my orders for me and for being the person I turn to when there is no clear answer. It took a while to figure out, but thanks for figuring out everything associated with making me a robotics student this past year. I especially enjoyed our random conversations. I won't forget our deal ;)

Finally, to everyone in TKE, it's been an awesome five years and while it would be fun to prolong growing up even longer, I really don't want to do a PhD. It's too bad I spent so much time at my desk and in my lab but I really cherished the rest of the time I got to spend with you guys. Spending time with all of you helped me escape my mountain of work. To my roommates Dave and Bennett, I'm so glad we got to live with each other this year and I know we'll be seeing much more of each other in the future. To my other "roommates" Costa, Sandro, Alex, and Lexa; thanks for always brining the fun to our room. I'm really going to miss everyone but I don't plan on being a stranger either.

Table of Contents

Table of Figures

Table of Tables

Chapter 1: Introduction

Since before Henry Ford invented the assembly line, people have been seeking to increase the efficiency with which goods are made. More recently, this has meant the introduction of automation and robotics into the factory. According to the International Federation of Robotics, there were 1.15 million industrial robots in use around the world with 166,000 new units shipped in 2011 [1]. The amount of new robots is expected to increase by 5% per year from 2013 to 2015 [1]. Unsurprisingly, the majority of these robots are used in the highly structured assembly lines of electronics and automotive manufactures [2]. This is because current industrial robots have been designed to be as stiff as possible to accurately and precisely repeat a few motions as quickly as possible [3]. For safety reasons, these robots also work completely separately from people [4]. While there is a large market for these types of devices, there are even more tasks which would benefit from a robot capable of handling dynamic and unstructured environments and able to work with humans. Current robotic technologies do not address this need.

For a robot to work in a dynamic environment, it must be adaptable. It must be capable of interacting with its environment without causing damage or being damaged. Furthermore, it must be aware of its surroundings instead of blindly repeating predetermined motions for hours if not days at a time. Therefore, the robot must have some form of compliance and sensory force feedback. Since the world has been shaped by humans, humans and even other animals provide a good basis to determine the best ways to incorporate compliance and sensory feedback into a robotic system.

Human joints have a natural elasticity to them which allows compliance with the outside world. It is because of this compliance that it is more common to overextend and sprain an ankle than it is to

break an ankle. Similarly, an easy way to demonstrate the compliance inherent in human joints is to examine the extension of a human finger. After having been fully extended, a finger can be push far past this joint limit without any pain or damage due the natural compliance.

Another key feature which compliance adds to a system is the ability to regulate force. While it may be relatively simple for a human to take a peg and push it into a hole, this task is very difficult for a traditional industrial robot unless the exact position of the peg and hole are known [3]. This is because traditional robots do not have the ability to provide a measured force or to adjust to their environment. While a high stiffness may be suitable for some industrial applications, there is clearly an advantage to having compliance and the ability to regulate force as shown by the human body. This thesis focuses on integrating compliant actuation into a robotic arm with tactile feedback.

Not only is the human body compliant, but it is also covered in sensors. Each of the five senses (touch, sight, taste, smell, and hearing) is an important sensor which provides information about the surrounds. The two of these most relevant to handling objects and therefore industrial applications are the senses of touch and sight. When working in an unknown and changing environment it is important to be able to see and feel what is going on. Vision is useful for providing an overall understanding of one's surroundings, while the sense of touch is often required for more delicate applications. For example consider trying to screw a nut onto a bolt while wearing gloves; vision is exactly the same but the decreased tactile feedback complicates the process. Additionally, while vision clearly simplifies the handling of goods, blind people demonstrate that it is not essential. Despite these facts, there has been much more research in the field of robotics on vision compared to tactile feedback [4]. Of the work that has been performed, much of it has been done for specific tasks under controlled conditions [5][6][7]. This is not well suited to the desired ability to work in unknown environments. However, the concept of sensitive manipulation [8][9][10] provides a more complete solution. Sensitive manipulation has

already been applied to the hands of robots [9] and more recently to the foot of a bipedal robot [11]. This thesis will continue with the expansion of sensitive manipulation and will apply it to the exterior of a robotic arm. While the complete project consists of a 6 degree of freedom (DOF) robotic arm coupled with a 4 DOF hand, this thesis focuses on the design, simulation, construction, and evaluation of the lower 4 degrees of freedom of this arm with an emphasis on compliant joints and the sensitive tactile shell.

1.1 Literature Review

Robotic arms have been and will continue to be an important topic for both robotic applications and research. This section performs the duty of providing a comprehensive review of the relevant history of robotic arms, series elastic actuators, tactile sensors, and control strategies. This section begins with a history of industrial robotic arms. It then moves into an examination of the two primary technologies for this thesis: series elastic actuators (SEAs) and tactile sensors. Finally, the literature review finishes with several case studies which examine a few crucial robotic arms.

1.1.1 History of Industrial Robotic Arms

According to the International Federation of Robotics, the first industrial robotic arm, called Unimate, was developed in 1959 by George Devol and Joseph Engelberger for their company Unimation [12]. The robot weighed 2 tons, could only be programmed in joint angles and had an accuracy of 1/10,000 of an inch [12]. The Unimate was designed with emphasis on accuracy associated with traditional robotic arms. A summary of the following 51 years is given in Table 1-1.

From Table 1-1, industrial robotics has followed a very iterative process and there have been very few large departures or technological innovation. Overall, it is a rather conservative industry in terms of raw technology. Therefore, despite the fact that this project has been designed for future

industrial applications, the most relevant technologies still remain in the research field. These include Justin [13], Domo [14], and Baxter [15] among others which will be examined in detail later in this chapter.

Table 1-1: Industrial Robot Milestones 1959-2010 (adapted from [12])

Year	Inventor	Accomplishment
1959	Unimation	First industrial arm
1961	Unimation	First industrial robot installed at GM. Stacked hot pieces of die cast metal
1962	AMF	First cylindrical robot
1967	Unimation	First industrial robot in Europe
1969	Unimation, GM	First spot welding robots. 90% of body welding automated.
1969	Trallfa	First commercial painting robot
1969	Unimation, Kawasaki	Kawasaki-Unimate 2000 first industrial robot in Japan
1973	N/A	3,000 industrial robots in operation
1973	Kuka	First robot to have 6 electromechanically driven axes
1973	Hitachi	First industrial robot with dynamic vision sensors for moving objects.
1973	Ichiro Kato	First full scale humanoid robot
1974	Bjorn Weichbrodt	First fully electric, microprocessor-controlled industrial robot
1974	Cincinnati Milacron Corporation	First minicomputer-controlled industrial robot
1974	Kawasaki	First arc welding robots.
1974	ASEA	First fully electric, microprocessor-controlled industrial robot
1975	Olivetti	First Cartesian-coordinate robot for assembly applications
1978	Puma	Puma created from Unimation and Vicarm
1978	Hiroshi Makino	SCARA Robot developed
1978	Reis	First 6-axis with own control system
1979	Nachi	First electromotor-driven robots
1981	PaR Systems	First industrial gantry robot
1981	Takeo Kanade	First Direct Drive Arm
1983	N/A	66,000 industrial robots in operation
1984	Adept	First direct-drive SCARA robot
1985	Kuka	First Z-shaped robot arm
1989	N/A	Unimation sold to Staubli
1992	Demaurex	First Delta robot packaging application
1998	ABB	FlexPicker, worlds faster picking robot, developed
1998	Gudel	First curved-track gantry and transfer system
1999	Reis	Integrated laser beam guiding
2003	N/A	800,000 industrial robots in operation
2004	Motoman	Improved robot control system. Synchronized control of 4 robots, 38 axis
2006	Comau	First wireless teach pendant
2006	Kuka	First “Light Weight Robot”
2010	Fanuc	First “Learning Control Robot”
2011	N/A	1.1 million industrial robots in operation

1.1.2 Series Elastic Actuators

As discussed in the beginning of chapter 1, significant compliance is an important aspect of manipulation which is currently neglected in most industrial robots. In fact, until recently the majority of the relevant research was actually focused on finding ways to reduce the compliance of the system [16]. This is because traditional approaches to robotics focused on making the system as stiff as possible to make them more precise [17]. Compliance can be added to a robotic arm either through hardware, with SEAs, or software with various control algorithms[18].

Most force control in robotic applications is done by monitoring the current of the motors [3]. If a spike in current is measured, the system knows that an outside force is acting upon the system. Similarly, by regulating the current and therefore torque of the motor, a robotic arm can provide a desired force at the end effector. However, there are limitations to this approach. Traditional motors are used in conjunction with a gearbox, allowing a low torque but high speed motor to have a high toque and low speed output. Unfortunately, gearboxes add significant friction to the system and result in large impedance due to the reflected inertia which increases by the square of the gear ratio [3]. Therefore, direct drive systems, even with current control, are ill suited for situations requiring high quality force control. This downside to direct drive systems, along with the many benefits of series elastic actuators resulted in the decision to use SEAs for this project.

The basic concept for a series elastic actuator is to add an elastic element between the motor/gearbox assembly and the load. A block diagram of an SEA is shown in Figure 1-1.

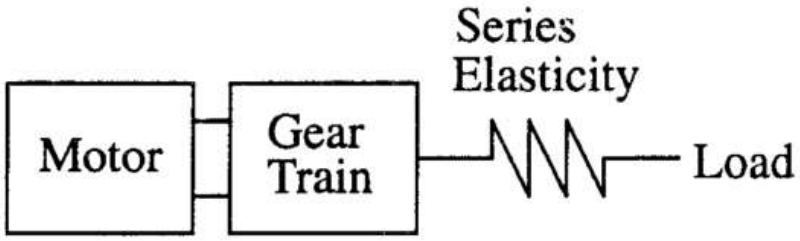

Figure 1-1: Series Elastic Actuator Block Diagram [16]

While this idea may be relatively new to the robotics industry, it is actually a close representation of how the suspension in a car works, where the car itself is separated from the road by an elastic element. One of the differences between the two systems is that a car suspension incorporates a damping element while SEAs do not currently have any damping. The other significant difference is that a typical car suspension is passive while an SEA is driven.

1.1.2.1 SEA Advantages

The key characteristics of an actuator are impedance, stiction, and bandwidth. Impedance is considered to be the force generated at the output due to load motion. The easiest way to think of this is that an easily back driven system has low impedance. Stiction is friction due to sliding contacts between mechanical components. Similar to static friction, a breakaway force is required before motion can occur, thereby setting a minimum for the force the actuator can create. Lastly, bandwidth is the frequency with which forces can be accurately commanded. The ideal actuator has zero impedance, zero stiction, and infinite force bandwidth. Muscle is the actuation technology which is closest to this ideal situation [3], while SEAs are a close man-made actuator and have low impedance, low friction, and decent bandwidth [3].

In addition to being close to the ideal actuator, SEAs have numerous other benefits. First and foremost, SEAs allow for a greater shock tolerance and act as a low pass filter reducing or eliminating vibrations felt by the gear train. They also have a lower inertia, better interaction with the environment,

allow for the use of more inexpensive gearboxes and motors, improve the stability of force control, and can store energy [3][16] [17].

1.1.2.2 Force Control

Series elastic actuators are very beneficial for force control applications from a controls point of view. This is because they take the often complex task of regulating force and transform it into a much simpler position control problem [16]. The force on the joint can be calculated using Hooke's Law using Equation 1, where F is the force on the joint, k is the stiffness of the elastic element, and Δx is the distance the elastic element has been compressed.

$$F = k * \Delta x \quad \textbf{1}$$

Therefore, instead of having to measure the motor current and relate it to a force, it has been reduced to a simplified linear equation. However, this means that the spring constant must be known, the deflection of the spring must be measured, and the location of the force must be known. When using traditional actuators, the dynamics of the total system is dominated by the inertia and friction of the actuators [17]. This is undesirable in applications such as robotic arms or walking robots where the dynamics need to be tightly controlled. Series elastic actuators can help reduces the effects and aiding in the controls of the system.

1.1.2.3 Primary Designs

There are three primary different design styles for series elastic actuators. The first, and original, uses torsion springs in a rotary manner [16]. The second uses a ball screw and compression springs to create a linear SEA [16]. The third is a hybrid version which uses compression spring but in a

rotary configuration [16]. There are several variations of these designs which will be discussed in the case studies.

Rotary SEAs rely upon custom torsion springs to provide their elasticity. Not only are these custom springs expensive, they are hard to fabricate and very stiff [16]. Because of this extreme stiffness, the SEAs exhibit minimal deflection and this deflection must be measured by strain gauges which are quite fragile [16]. One advantage of torsion springs is that they can be much smaller than the alternatives and can be directly mounted to the motor shaft. A schematic of this configuration is shown in Figure 1-1.

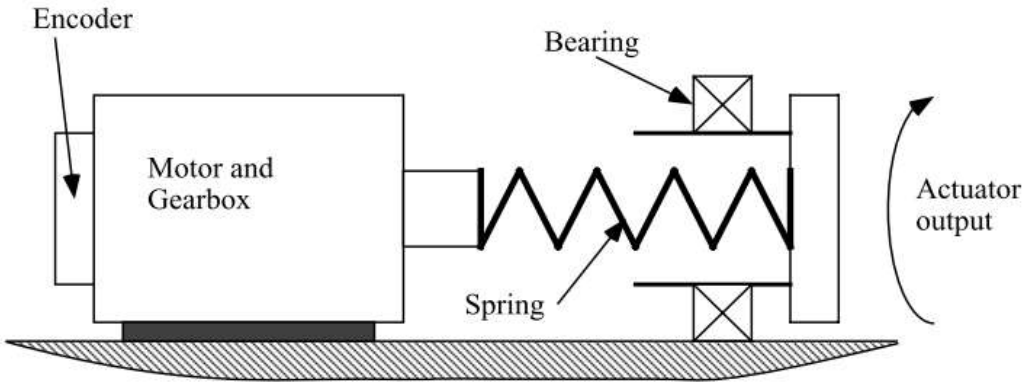

Figure 1-2: Torsion Spring SEA [16]

From Figure 1-2, the motor and gearbox are fixed to the previous link. The torsion spring is used as a coupler between the output shaft of the gearbox and the output of the actuator. The bearing is there to ensure linearity and to add support. In addition to the spring itself being much smaller, this configuration also has good modularity since it can be its own module attaching to the gearbox and the actuator.

The second configuration uses a combination of linear rails and a ball screw to create a linear series elastic actuator. The precision required for linear motion in the rails and ball screw results in a large and expensive system [16]. An example of this version is shown in Figure 1-3.

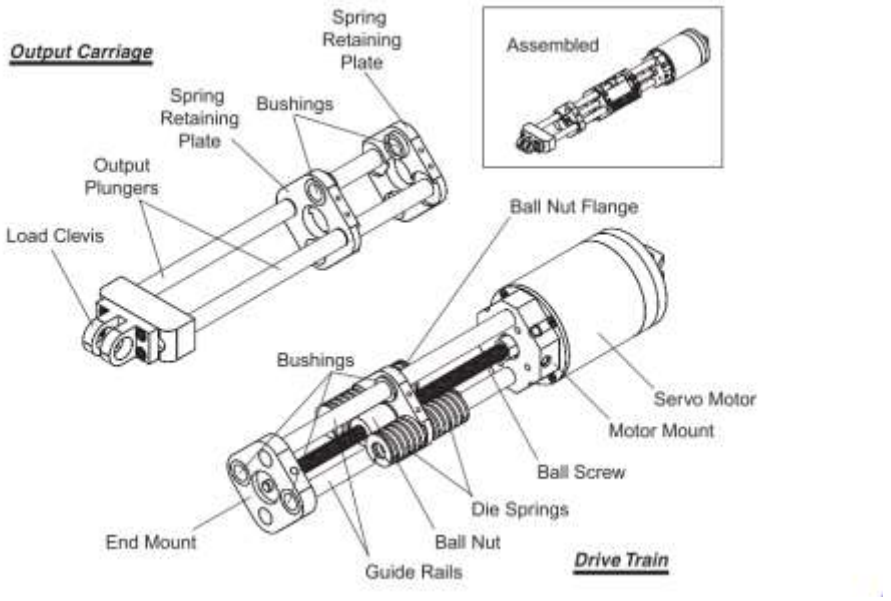

Figure 1-3: Linear SEA Assembly [3]

From Figure 1-3, the springs of the drive train fit in between the spring retaining plates of the output carriage. Therefore, a pushing force on the load clevis results in the lower set of springs being compressed while a pulling force results in the upper set of springs being compressed. When assembled and under no force, each spring is half compressed. Therefore, when one side is fully compressed, the other is completely uncompressed but still constrained. Like the rotary option, this configuration provides good modularity as the SEA system can be directly attached to the motor and then to the load. However, it is a much larger configuration than the rotary option.

The last configuration is a hybrid of these two approaches. The elastic element is provided by compression springs which exhibit a linear force; however, this force acts on a cable which translates the force to a rotary joint. Therefore, it has a linear elastic element in a rotary package. This configuration is shown in Figure 1-4.

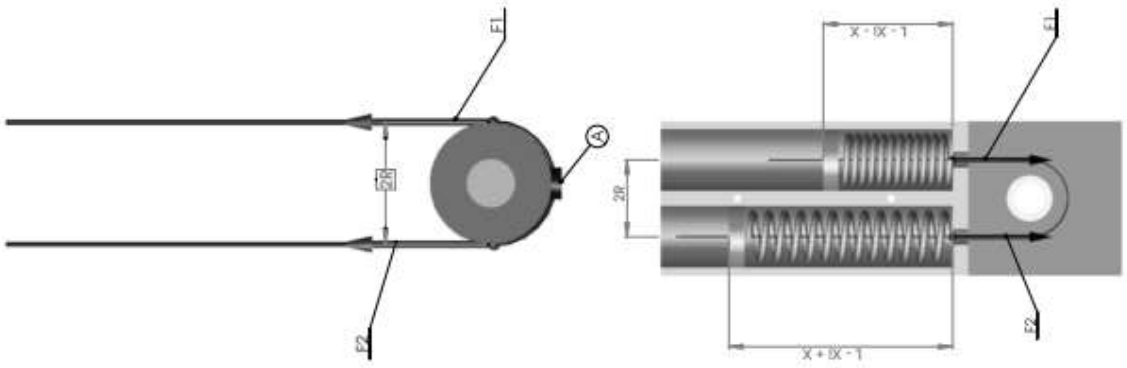

Figure 1-4: Hybrid SEA [19]

Figure 1-4 depicts both the spring mechanism and the rotary pulley. The pulley is actually shown in a cutaway view as shown by the labeled F1 and F2. Like the linear configuration, the springs are at half compression when no force is acting upon the system, however, for this figure the top spring is completely compressed while the bottom spring is completely uncompressed. The primary advantages of this approach are that it uses off-the-shelf springs and does not require expensive linear rails or ball screws [19]. However, while it is modular and scalable, it cannot be as tightly packaged as the torsion spring. That being said, it is a much smaller option than the purely linear configuration.

An important modified form of this last configuration is worth noting here. The bipedal walking robot Caminante uses a form of this configuration of SEAs in its legs [11]. However, it built the SEAs directly into the joints instead of as separate modules as seen in Figure 1-5.

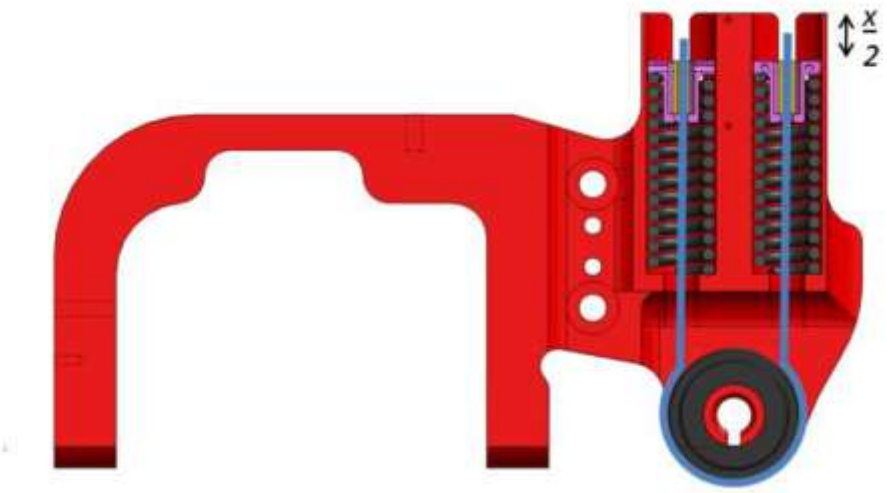

Figure 1-5: Integrated SEA [11]

While this design may one day evolve to the point where the links themselves act as the elastic element, they proved quite troublesome for assembly [11]. This is because the springs have to be compressed while on the robot, limiting the tools available. It is done by using the motor to fully compress one of the springs while the plug is attached to the other spring. When the motor is powered off, the system moves to equilibrium. Ultimately, the system had to be tensioned by using the motor to provide an external compressive force. It also meant that there was always a significant amount of tension in the cable (1/2 total spring force). This is because the half compression of the springs traveled through the entire joint system instead of the series elastic element. Lastly, this approach reduces the modularity of the system and results in a custom SEA solution for each joint.

1.1.2.4 SEA Summary

As has been shown in the previous section, series elastic actuators provide a clear benefit over traditional actuation technologies. This is especially true when the device has a high likelihood of having unexpected collisions, being used for force control, or working with or near humans [3] [16] [16]. Since the arm developed for this thesis is being designed for such situations, it will incorporate some version

of SEAs in each joint. There are also three different primary configurations for SEAs, each with their own advantages and disadvantages [3] [16] [19] [11]. Given the need for modularity and low cost, an instantiation hybrid version of the SEA is used in this work.

1.1.3 Tactile Sensors

Tactile sensing is a field which has been researched in both natural and man-made fields of research and has been found to be very important for manipulation. The importance of force sensing can be most easily seen in humans. For example, when anesthetized, human fingers become clumsy due to the lack of feedback [20]. Furthermore, while rare in robotics, almost all animals exhibit full-body tactile sensing, suggesting that it is beneficial for operating in unstructured environments [21]. However, for tactile sensing to be effective in robotic situations, it must be robust yet still flexible and easily deflect when contacting an object. First, an analysis of how humans feel is performed, followed by an examination of the current methods used in the field of robotics. Furthermore, as this thesis focuses on the integration of tactile sensors, instead of the development of new sensors, the functionality of both the human skin and tactile sensors for robotic systems are only covered at a high level.

1.1.3.1 Human Tactile Sensing

Bio-inspired robots are becoming increasingly more common and a significant amount of these robots draw their motivation from humans. In the case of tactile sensing, humans prove to be a very good source of inspiration as human skin is an adaptable and robust sensor capable of feeling a wide range of forces. The mechanoreceptors in the human skin, shown in Figure 1-6, are capable of detecting several different properties including shape, size, texture, temperature, and position [9].

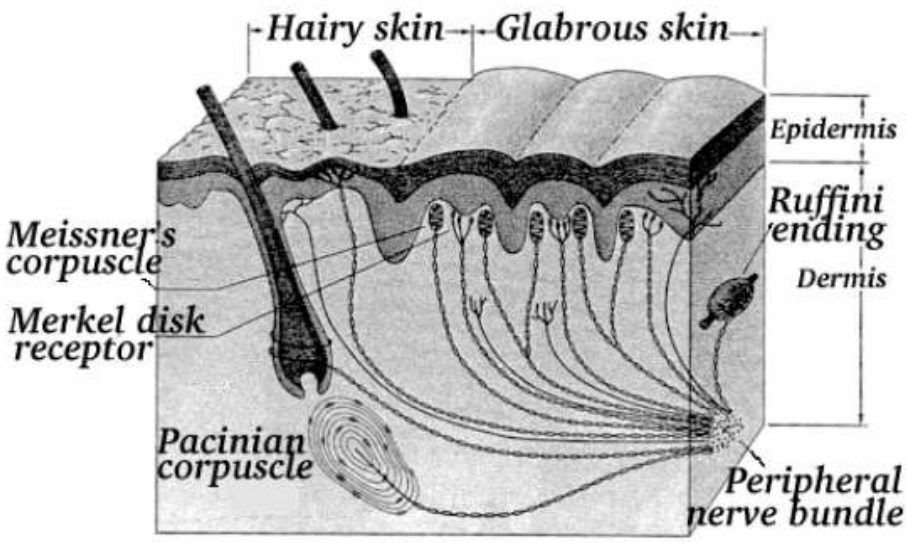

Figure 1-6: Mechanoreceptors in Human Skin [9]

As shown in Figure 1-6, skin with hair and skin without hair have different methods for sensing. The important aspect of hairless skin is the fact that it is comprised of several different types of sensors where one is highly sensitive but saturates quickly, another is much slower reacting and measures the strain in the skin, a third responds to rapid indents but cannot handle pressure, and lastly a slow reacting sensor [9]. Skin with hair in it follows a similar approach but only has two types of sensors which detect the movement of the hair and stretching of the skin [9]. In reality, these receptors are actually several sensors in one. Therefore, the mechanoreceptors may not be able to be directly replicated in a man-made system.

In addition to how the sensors function, it is important to examine the resolution of the human skin. The resolution actually varies intelligently depending upon the location of the body such as shown in Figure 1-7. As expected, the fingers have the finest resolution at less than 5 mm since they perform the majority of dexterous manipulation. Similarly, larger extremities such as the thigh, back, calf, or arm have a much higher resolution of around 40 mm. These numbers were determined experimentally by pricking subjects in these locations with two pins to see if it registered as one or two pricks. The number represents the distance between the two pins when they registered as separate pokes [22].

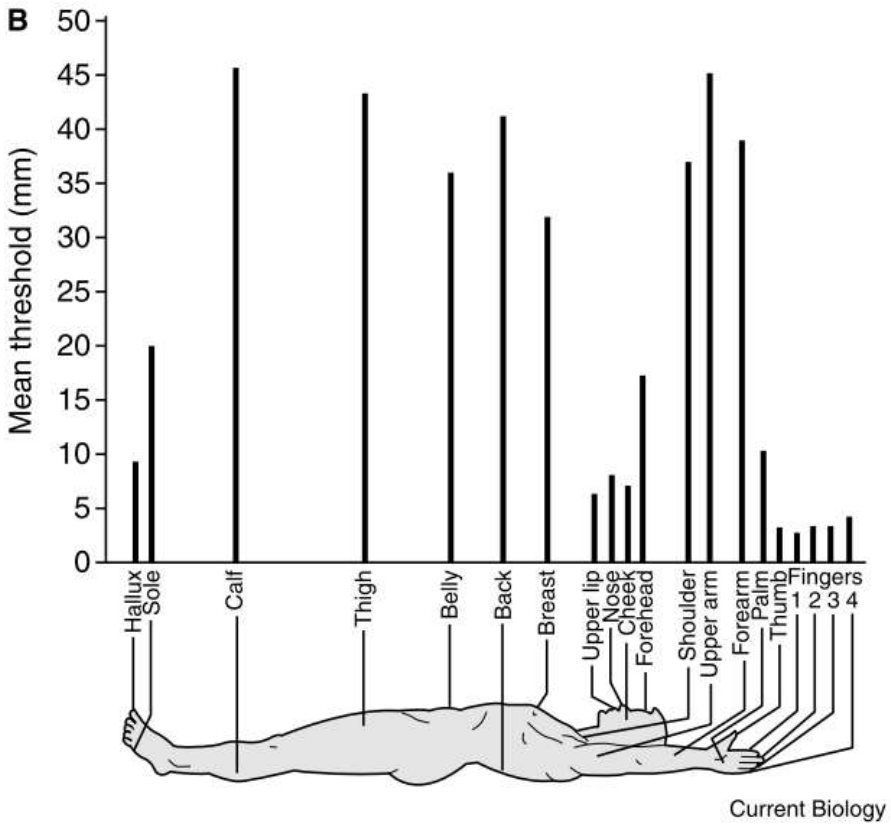

Figure 1-7: Tactile Spatial Resolution of the Human Body [22]

Since this project focused upon developing an arm, the most important areas are the shoulder (36 mm), upper arm (46 mm), and the forearm (40mm). Therefore, the resolution of the tactile sensors should be approximately 40 mm to replicate a human being. Since there is limited relevant work on the topic of increased tactile sensing, the human body provides a good baseline to determine the balance between adequate feedback and information overload.

1.1.3.2 Robotic Tactile Sensing

The different methods for incorporating tactile feedback into robotics has been extensively investigated and has resulted in a several different technologies [23]. These technologies include strain gauges, force sensing resistors [24], piezoelectric sensors [25], optical sensors [26], magnetic sensors [9], and more. More information about all of the different types of tactile sensors can be found in [23]. This

analysis will focus on a method developed by Dr. Eduardo Torres-Jara which proves to be a more complete approach to manipulation using tactile feedback in an unstructured environment. His approach has been applied to the hands of the robotic platforms Obrero [9] and GoBot [8], and the feet of the robot Caminante [11]. Obrero, shown in Figure 1-8, is a humanoid robot developed to manipulate unknown objects and is shown in Figure 1-8, while GoBot, shown in Figure 1-9, was specifically developed to play the Japanese game Go. Caminante, shown in Figure 1-10, was developed to investigate the impact of increased tactile feedback on walking.

Figure 1-8: Obrero Robot [9]

Figure 1-9: GoBot Robot [8]

Figure 1-10: Caminante Robot [11]

On all of these robots, the sensor arrays are the green pads. Each pad contains multiple domes which each house one sensor. Obrero uses a magnet implanted in the dome of each sensor in conjunction with four hall-effect sensors to determine the magnitude and direction of a deformation of the dome. While this proved effective, it meant that ferrous materials would affect the sensor performance. Therefore, GoBot uses an infrared LED and four phototransistors to measure the diffraction off of the dome as shown in Figure 1-11. Caminante uses this same principal but in a smaller

package due to advances in electronic technology. This project will extend this technology further by integrating the sensors into the arm of a robotic platform.

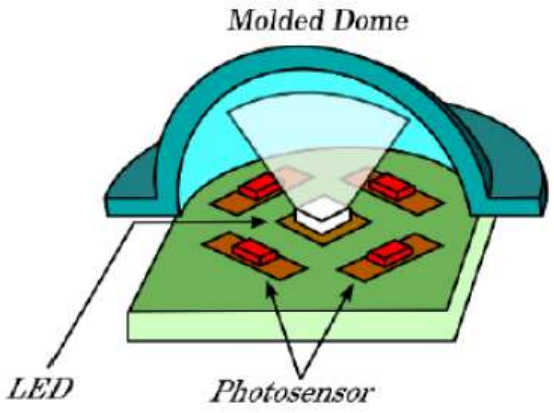

Figure 1-11: Optical Tactile Sensor [11]

1.1.3.3 Impact on Control Schemes

The last aspect to consider about tactile sensors is the impact they can have on the controls of a robot. This arm is being developed to operate safely in unknown environments. It has series elastic actuators for compliance and for force control. However, the SEAs can only be used to regulate the force; the location of the force must be known in order to create a measured force. This is the role the tactile sensors play.

The original use of tactile sensing to impact the control of a robot was performed in [9] and expanded upon in [8]. These two works developed a new approach to controlling a robot called sensitive manipulation. The concepts developed and lessons learned on these robots were applied to the development of the arm for this thesis, however, did not have tactile sensors incorporated onto the arms of the robots.

There has also been research performed in this field to use a form of tactile skin on a robotic arm to determine forces. The first utilized the skin to detect contact locations and attempted to determine

the external wrenches being applied to the system [27]. The added tactile feedback was used to generate a more complete representation of the dynamics. The focus of this work was on determining external forces and did not investigate methods for motion planning based upon this information.

Additional research has been performed which focused on utilizing force feedback to manipulate objects in cluttered environments [21]. This research focused on the motion planning aspects of having increased knowledge thanks to force feedback on the arm. It utilized a pre-existing arm with tactile sensors and does not have the ability to manipulate objects. Additionally, it is currently a large and bulky system as shown in Figure 1-12.

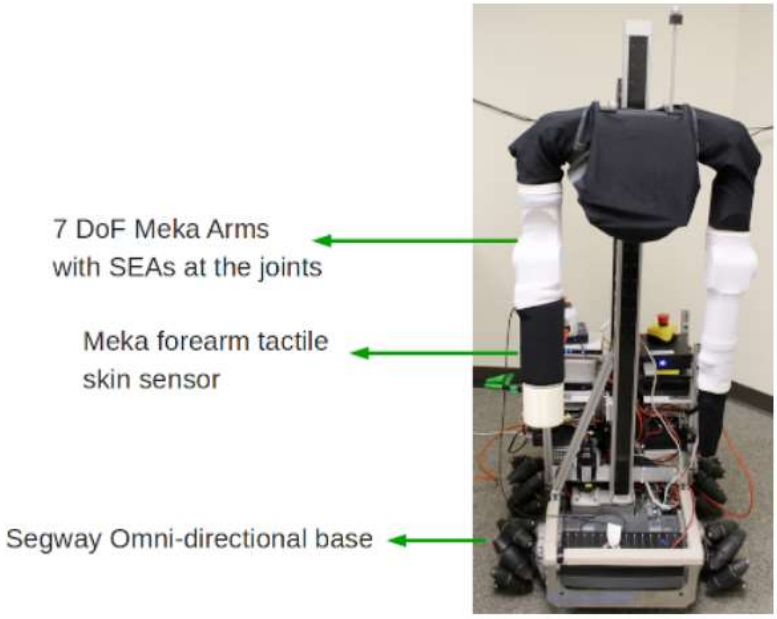

Figure 1-12: Meka Arm with Tactile Skin [21]

While the system shown in Figure 1-12 is quite similar to the arm developed for this work, there are several key differences. The primary difference is related to the sensors used. The capacitive sensors used in [21] only detect normal forces while the sensors used on this arm can also detect shear forces. Shear force can provide valuable information about the environment and contact state allowing the robot to form a better understanding of the situation and therefore react more appropriately.

Additionally, the complete arm (consisting of the work performed for this thesis as well as by others) will be focused on manipulation with whole arm tactile feedback acting as a significant feature instead of the core functionality. Finally, while it is possible the navigation algorithms developed in [21] can be extended to include human interaction, human-robot-interaction is one of the primary concerns for this arm.

1.1.4 Case Studies

The following case studies aim to highlight the most advanced robotic arms which incorporate series elastic elements and/or tactile sensing. The first, Justin [13], was designed as a research platform to investigate two handed manipulation and uses its own form of variable resistance series elastic actuators. The next example, Domo [28], was developed at MIT to experiment with robot manipulation in unstructured environments. It is also closely related to the robot Obrero which was discussed in regard to tactile sensors. Baxter [15] is the first industrial robot with SEAs to be mass produced. Lastly, as a departure from the concept of industrial robots, an intelligent and motorized prosthetic arm is examined [29]. The goal of these case studies is to provide an overview of the more influential systems and to provide a better view for how this thesis fits into the world of robotic arms.

1.1.4.1 DLR/Justin

The robot Justin, shown in Figure 1-13, is being developed by the German Aerospace Center (DLR) to investigate two handed manipulation and allow robot telepresence in space. As such, it is quite similar to the robot Robonaut, shown in Figure 1-14, developed by NASA and examining Justin will also cover the important features of Robonaut [30][31].

Figure 1-13: Justin Robot [32]

Figure 1-14: Robonaut 2 Robot [31]

Justin has 43 degrees of freedom and is able to carry payloads of 15 kg while having a total mass of 45 kg [32]. Justin actually does not use series elastic elements while Robonaut 2 and the more advanced version of Justin's arms, DLR Hand Arm System [33] [34], do. Instead, Justin uses torque sensors in each of the joints to implement highly sensitive torque and impedance controllers [13]. This approach takes a software solution while SEAs take a hardware approach. This allows for Justin's mechanical design to be less complex since elastic elements are not required. However, the controls become more complicated to implement and the torque sensors are still rather expensive in order to have accurate measurements.

DLR has also developed its Hand Arm System which is unique because the elastic elements can have a variable stiffness [33]. This is very beneficial from a controls point of view as the stiffness can be tailored to the task at hand. It works by using two cam rollers to adjust the compression of a spring. The disadvantage to this system is that it requires two actuators per joint: the actuator to move the joint and the actuator to adjust the cams. This setup is shown in Figure 1-15.

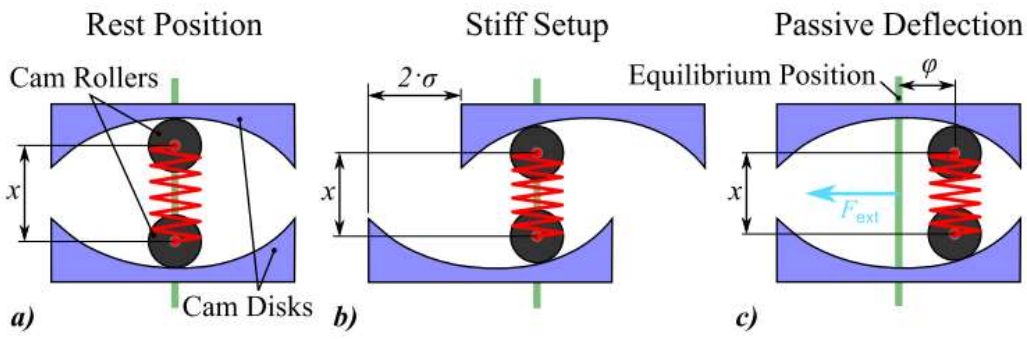

Figure 1-15: Variable Stiffness SEA [33]

1.1.4.2 Obrero

Obrero is the most recent of several robots developed by MIT utilizing series elastic actuators. Obrero's predecessors include Domo [28], Cog [35], and Kismet [36]. Domo also served as the basis for the design of Obrero [9], where tactile sensors were applied to the hand to first investigate sensitive manipulation. The two robots are shown in Figure 1-16 and Figure 1-17.

Figure 1-16: Domo Robot [37]

Figure 1-17: Obrero Robot [38]

Domo and Obrero utilized linear style SEAs in the body and arm. Domo is one of the few robots to reveal its spring rates. The springs in the arm have a rate of 91 kN/m while the springs in the hand have a rate of 21 kN/m [14].

Obrero is significant because of the successful integration of the hybrid SEAs in the fingers along with the tactile sensors on the fingers and palm [39]. It was the first robot to develop sensitive manipulation and is the basis for this project. However, the tactile sensors were only used on the end effector. It is also important to note the control strategy used on Obrero. Obrero was able to use the same algorithm to grasp several different unique objects without any existing knowledge of these objects. It was able to do this thanks to the many advantages of the tactile sensors coupled to the compliant fingers.

1.1.4.3 Baxter

Unfortunately, there is not much information available about Baxter [15], shown in Figure 1-18. Baxter is unique because it is the first commercially available industrial robot with series elastics. More importantly, from a commercial point of view, Baxter is considered to be the first low price industrial robot at only $22,000. Baxter is capable of manipulating payloads up to 2.3 kg and move at unloaded speeds of up to 1 m/s. Another unique aspect of Baxter is that it can enter a teach mode where an operator moves Baxter's arms to teach it a new operation. Lastly, the incorporation of SEAs makes Baxter safe to work near humans and does not need to be in a separate area. Baxter is capable of doing this by measuring the external forces on the arm and attempting to set the force equal to zero, causing Baxter to follow the user effortlessly. As a result of these and other features, Baxter is considered the cheapest and easiest to use industrial robot on the market.

Figure 1-18: Baxter Robot [15]

1.1.4.4 Prosthetic Arm

Dr. Todd Kuiken has been working on developing more advanced prosthetics. His most recent work, detailed in a TED Talk [29], has focused on relocating the nerves of a missing arm into the chest. Doing this allows the muscles of the chest to act as a biological amplifier. The prosthetic arm can then measure the movement of these muscles to command the arm to move, allowing for much more intuitive control of the prosthetic. An interesting side-effect of this approach is that the patient also gained hand sensations in the chest [29].

The ability to regain sensation creates a huge need for a robotic arm for greater sensitivity. The patient currently has the ability to feel but there are no arms which can provide any significant sensory feedback. While this project is primarily focused on industrial applications, it is well suited to a future use in prosthetics where mechanical arms must have compliance to replicate a human arm, but must also have sensitivity to provide valuable feedback to the patient which is sorely lacking in current designs.

1.2 Thesis Contribution

This thesis develops a platform with which to research control algorithms to best utilize tactile feedback in unknown and changing environments. These algorithms will incorporate force control not only of the end effector but also the arm itself to manipulate a diverse range of objects. While tactile sensors and compliant arms have been researched separately, they have not been integrated into a harmonious system. The closest known research was that in [21] which combined two separate systems and did not perform any manipulation. It was also solely focused on the control algorithms and software. No information is available on the design of the arm or tactile sensors. This thesis, on the other hand, is focused on the development of a sensitive and compliant platform. Therefore, the emphasis is on the design choices and construction of the arm.

This thesis focuses on the mechanical design, analysis, and construction of the first 4 joints of a 6 DOF robotic arm. The last two degrees of freedom, the hand, and the electronic and software architecture are not the focus of this particular thesis and therefore will receive only minor attention. It has been found that there are few resources which properly detail the complicated process for selecting the elastic elements or actuators for a system with series elastic actuators. Therefore, another of the contributions of this thesis is a detailed guide on the proper method for selecting the elastic elements and actuators which can be followed for any device with series elastic actuators. The final contributions of this thesis are a new configuration of a series elastic actuator along with a novel integration of the hybrid form of SEA.

1.3 Thesis Layout

The remainder of this thesis is organized to cover the simulation, design, control, assembly, and testing of the robotic arm. Chapter 2 covers the kinematic and dynamic models of the arm. Chapter 3 details the mechanical design of the arm including the design requirements and justification for design

decisions. It is during this chapter that the methods for selecting the springs and actuators are discussed based upon the results of the dynamic model. Chapter 4 proposes methods for performing force control and motion planning using this platform. Chapter 5 includes the assembly and testing of the relevant portion of the arm. Chapter 6 concludes the thesis and suggests future work on the project.

Chapter 2: Kinematics and Dynamics

This chapter reports the kinematic and dynamic models of the arm shown in Figure 2-1. Therefore, they are for a 6 DOF arm instead of only the 4 DOF developed for this project, but neglect the degrees of freedom in the hand. The chapter begins with an introduction of the Denavit-Hartenberg (D-H) parameters which will be used for both the kinematics and dynamics. Next, the forward and then inverse kinematics of the system are detailed. Lastly, the dynamic model is discussed along with the tests performed using the dynamic model.

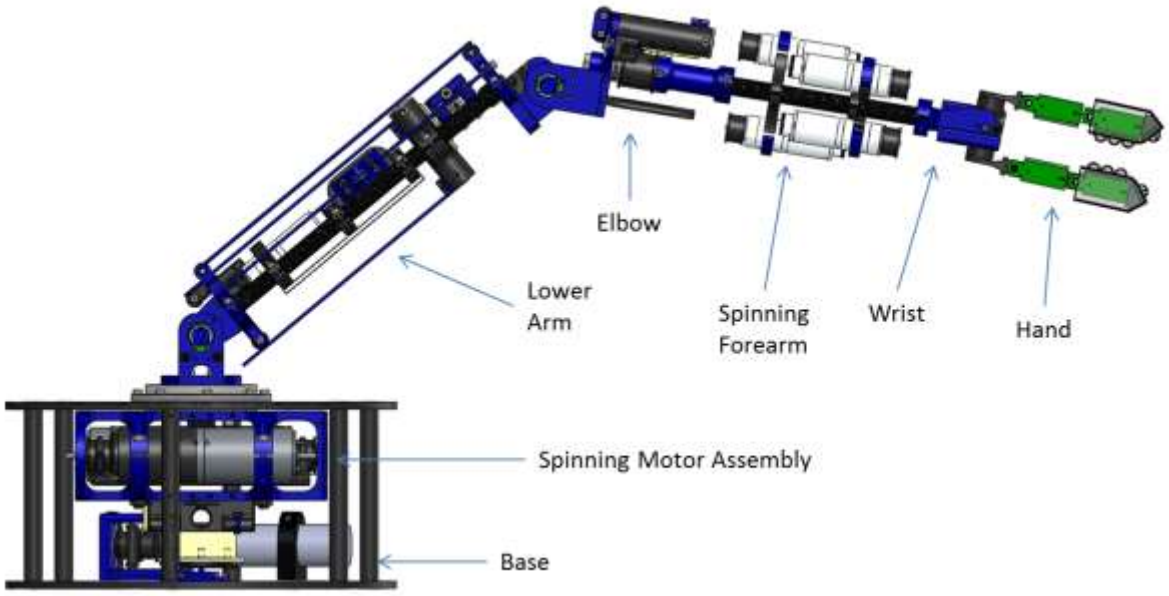

Figure 2-1: 6 DOF Arm

This chapter primarily serves as a background of the concepts needed for kinematic and dynamic modeling. The specific forward and inverse kinematics for this arm are covered and the dynamic model developed is used in Chapter 3 to aid in the selection of the motors and springs for the arm.

2.1 Denvit-Hartenberg Parameters

Robotic manipulators can be lumped into two groups: serial and parallel. A serial manipulator has the first link connected to the ground plane and the last link acting as the manipulator with all other links connecting the two. A parallel manipulator has all links connected to the ground plan and the manipulator. Robots may comprise of revolute (rotational) and prismatic (translational) joints. This arm has six revolute joints. The D-H parameters can be used to describe the relationship between joints in a generic way. Transformation matrices can then be created which can be used to determine the location of any of the joints based upon the previous joint angles. D-H parameters rely upon assigning the coordinate frames of each link in a specific manner. The coordinate frames for this robotic arm are shown in Figure 2-2. However, only the Z axes are shown for clarity. The four key parameters for D-H can be determined for each joint: θ, α, d, and a. θ is the joint angle, α, the link twist, d the link offset, and a the link length. The table of D-H parameters for this arm are shown in Table 2-1. It is important to note that a q represents an actuated joint and that these parameter have been set such that the zero height is at Z_1 instead of the bottom of the base.

Table 2-1: Denavit-Hartenberg Parameters

Joint	$\theta\ (radians)$	d (meters)	a (meters)	$\alpha\ (radians)$
1	$q1$	0	0	$\frac{\pi}{2}$
2	$q2$	0	0.304	0
3	$q3 + \frac{\pi}{2}$	0	0.021	$\frac{\pi}{2}$
4	$q4$	0.314	0	$-\frac{\pi}{2}$
5	$q5 - \frac{\pi}{2}$	0	0	$\frac{\pi}{2}$
6	$q6$	0	0	$\frac{\pi}{2}$

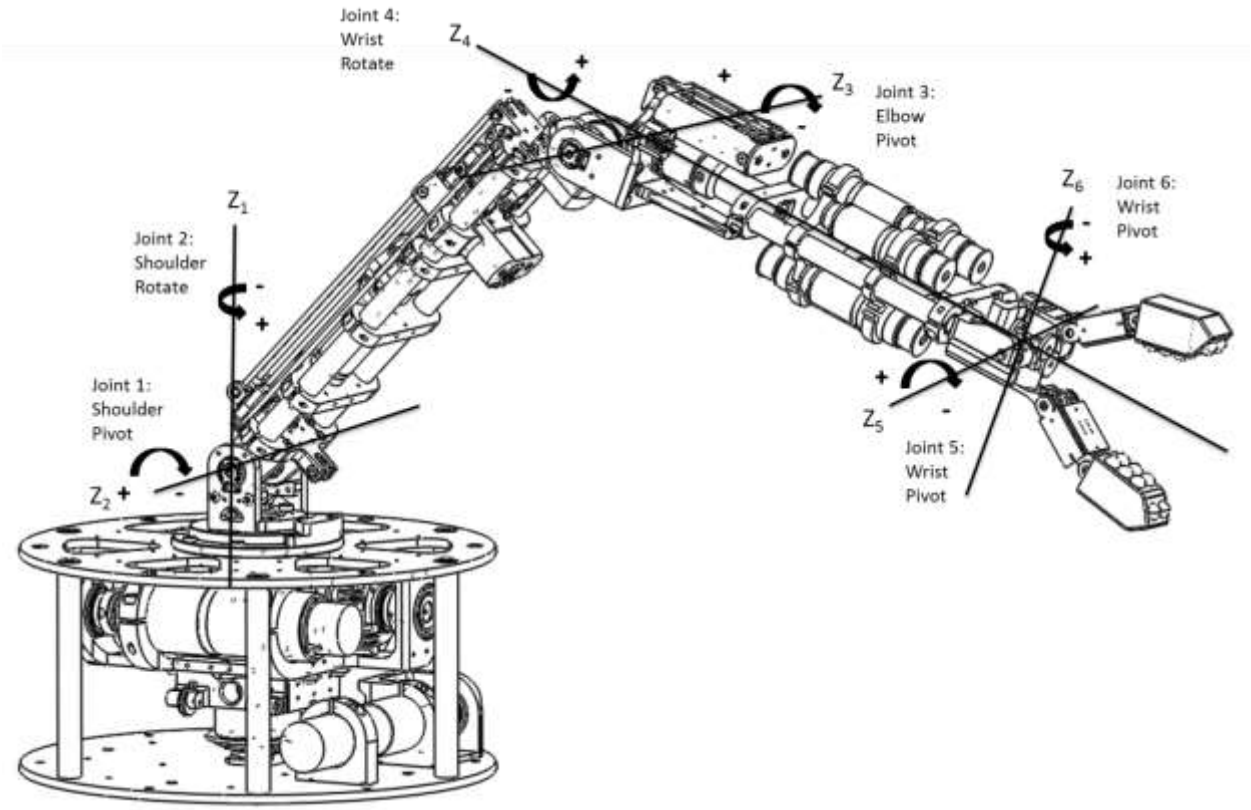

Figure 2-2: 4 DOF Arm Coordinate Axes

2.2 Forward Kinematics

Each joint can represented as a number from 0 to *n*, where 0 is the ground link and *n* is the end effector location. Additionally, the position and orientation of each joint can be determined based upon the previous joints using transformation matrices. These movements can be broken down to four basic movements: translation along z (Equation 2), translation along x (Equation 3), rotation about z (Equation 4), and rotation about x (Equation 5). Translation along y and rotation about y are not allowed by the D-H parameters and therefore are not necessary for this transformation matrix.

$$Translation_z = \begin{bmatrix} 1 & 0 & 0 & 0 \\ 0 & 1 & 0 & 0 \\ 0 & 0 & 1 & d_i \\ 0 & 0 & 0 & 1 \end{bmatrix} \quad \textbf{2}$$

$$Translation_x = \begin{bmatrix} 1 & 0 & 0 & a_i \\ 0 & 1 & 0 & 0 \\ 0 & 0 & 1 & 0 \\ 0 & 0 & 0 & 1 \end{bmatrix} \quad \textbf{3}$$

$$Rotation_z = \begin{bmatrix} \cos\theta_i & -sin\theta_i & 0 & 0 \\ sin\theta_i & cos\theta_i & 0 & 0 \\ 0 & 0 & 1 & 0 \\ 0 & 0 & 0 & 1 \end{bmatrix} \quad \textbf{4}$$

$$Rotation_x = \begin{bmatrix} 1 & 0 & 0 & 0 \\ 0 & \cos\alpha_i & -sin\alpha_i & 0 \\ 0 & sin\alpha_i & cos\alpha_i & 0 \\ 0 & 0 & 0 & 1 \end{bmatrix} \quad \textbf{5}$$

The full homogeneous transformation matrix, A_i, is the product of these four basic transformations and is shown in Equation 6.

$$A_i = \begin{bmatrix} \cos\theta_i & -\sin\theta_i \cos\alpha_i & -\sin\theta_i \sin\alpha_i & a_i\cos\theta_i \\ 0 & \cos\theta_i & -\cos\theta_i \sin\alpha_i & a_i\sin\theta_i \\ 0 & sin\theta_i & cos\theta_i & d_i \\ 0 & 0 & 0 & 1 \end{bmatrix} \quad \textbf{6}$$

Furthermore, the homogeneous transformation matrix can be decomposed as shown in Equation 7, where $R \in \mathbb{R}^{3x3}$ is the rotation matrix and $P \in \mathbb{R}^{3x1}$ is the position matrix.

$$A_i = \begin{bmatrix} R & P \\ 0 & 1 \end{bmatrix} \quad \textbf{7}$$

However, A_i only describes the ith joint in terms of the i-1th joint. Therefore, this must be back propagated to whichever joint the ith is to be defined from (defined as j, but typically joint 0) to produce the complete transformation matrix ${T_j}^i$ as shown in Equation 8.

$$T_n{}^j = \prod_{i=j}^{n} A_i\,(q_i) \qquad \textbf{8}$$

Equation 8 was then applied to determine the position of each joint from the ground based upon the joint angles. Since the reference frame was set to be at the Z_1 axis, an offset was added to account for the height of the base. A MATLAB based simulation was the developed showing accurate link lengths and correct coordinate frames. The result of this simulation is shown in Figure 2-3 and the MATLAB script is shown in Appendix A.

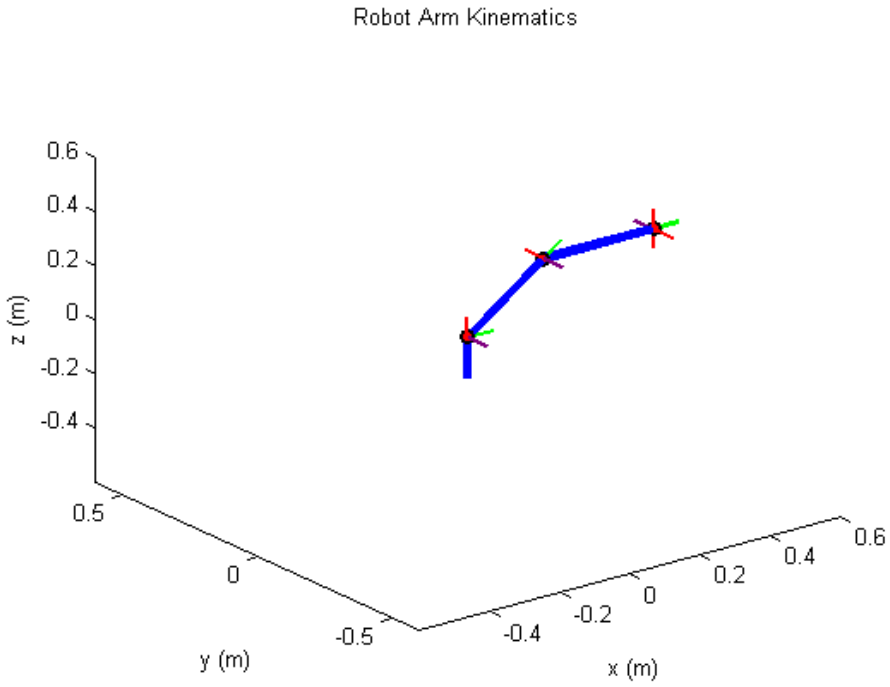

Figure 2-3: Forward Kinematics

Figure 2-3 shows the arm with joint angles of 0, 45, -45, 0, 0, and 0 degrees. Given these angles, the position of each of the joints can be known. Most importantly, the end effector position and orientation is now known. Next, for the inverse kinematics, the opposite of this will be performed. A desired position and orientation will be provided and the inverse kinematics will calculate the required joint angles.

2.3 Inverse Kinematics

Inverse kinematics allows for a system to be commanded to a desired position and orientation. This is beneficial for manipulation because most of the time you want an arm to go to a specific location and do not know what the joint angles need to be. Inverse kinematics takes the desired position and orientation and derives the necessary joint angles. Unfortunately, unlike forward kinematics, there is no general formula that can be used to solve the inverse kinematics for all systems. This is because there is often more than one solution for any given pose. For example there are 6 degrees of freedom in space so any manipulator with more than 6 degrees of freedom will be redundant and have multiple possible solutions. Furthermore, there is the choice between having the elbow be up or down. An illustration of this kinematic redundancy is shown in Figure 2-4.

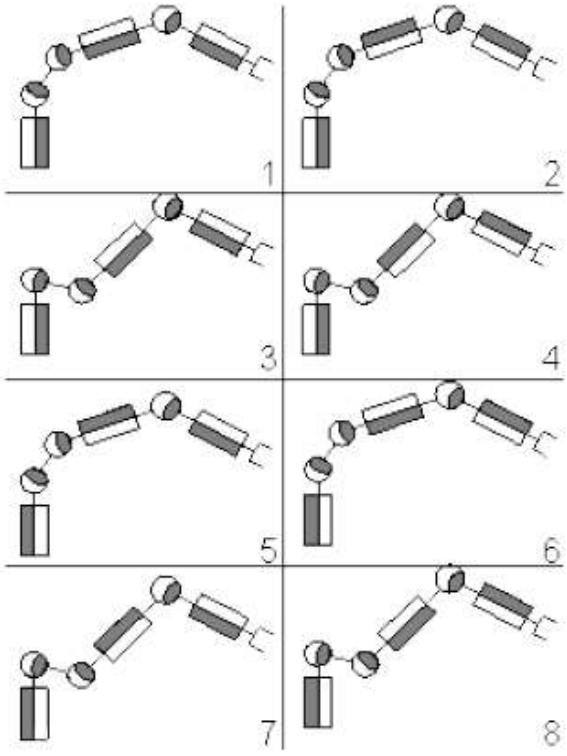

Figure 2-4: Kinematic Redundancy in an Arm [40]

As shown in the figure, several configurations all have the same position. This can be beneficial and the optimal configuration can be chosen based upon extra criteria, such as avoiding singularities or the limits of the arm. Since the full arm has 6 degrees of freedom, it will not have redundant joints but it will have the choice between having the elbow up or down such as shown in segments 3 and 5 of Figure 2-4.

The strategy of kinematic decoupling [41] will be used on this arm. For this approach, the arm is split into a 3 DOF arm and a 3 DOF wrist. This can be done because the z axes of the last three joints of the arm intersect. The first 3 DOF (shoulder and elbow) can then be determined based on the position and the last three can be used to satisfy the orientation requirements.

2.3.1 Inverse Position

The first three joints can then be solved geometrically based upon the figure below.

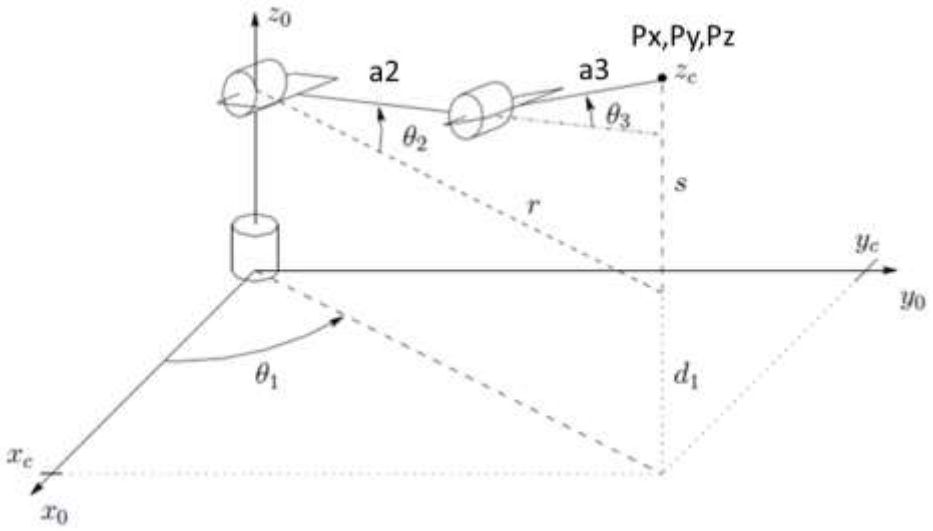

Figure 2-5: 3 DOF Elbow Manipulator Inverse Kinematics (modified from [41])

First, the tip position (Px,Py,Px) can be calculated symbolically using forward kinematics. This results in Equations 9, 10, and 11.

$$P_x = -C_1 * (a_3 * S_{2+3} - a_2 * C_2) \quad (9)$$

$$P_y = -S_1 * (a_3 * S_{2+3} - a_2 * C_2) \quad (10)$$

$$P_z = a_2 * C_{2+3} + a_2 * S_2 \quad (11)$$

As shown in Figure 2-5, θ_1 is the easiest joint to solve for using Equation 9.

$$\theta_1 = \tan^{-1}\frac{y_c}{x_c} \quad (12)$$

θ_2 and $\theta_3$can be found using the information shown in Figure 2-6 and Equations 13 and 14 which define s and r. Note that for this case $d_1 = 0$ because of how the base frame was defined.

$$r = \sqrt{x_c^2 + y_c^2} \quad (13)$$

$$s = z_c - d_1 \quad (14)$$

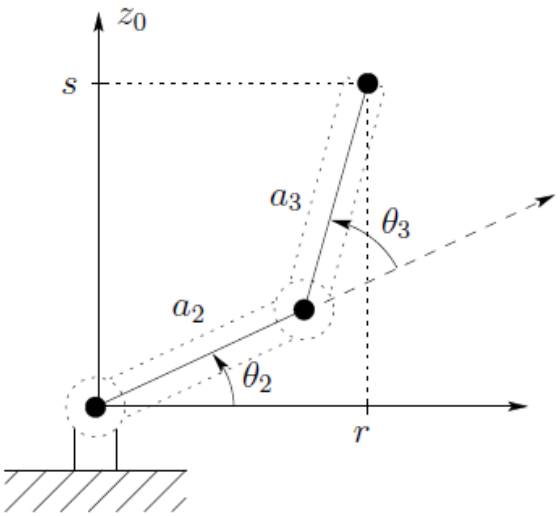

Figure 2-6: Planar Inverse Kinematics[41]

θ_3 can be determined by first using the law of cosines on Figure 2-6, resulting in Equation 15.

$$C_3 = \frac{r^2 + s^2 - a_2^2 - a_3^2}{2 * a_2 * a_3} \quad (15)$$

Next, Equations 13 and 14 can be substituted into Equation 15, creating Equation 16.

$$C_3 = \frac{x_c^2 + y_c^2 + (z_c - d_1)^2 - a_2^2 - a_3^2}{2 * a_2 * a_3} = D \quad \textbf{16}$$

Using this intermediate variable D and the knowledge that $sin^2 + cos^2 = 1$, results in the solution for θ_3 which is shown in Equation 17.

$$\theta_3 = atan2(D, \mp\sqrt{1 - D^2}) \quad \textbf{17}$$

Notice that θ_3 has two different answers. One is the elbow up configuration while the other is elbow down. In general, the elbow up configuration will be used; however, occasionally elbow down will be required.

Lastly, θ_2 can also be determined using the law of cosines. Firstly the intermediate step δ is calculated using Equation 18 and then $\theta_2$is found in Equation 19. Remember that r is defined in Equation 13 and s is defined in Equation 14.

$$\delta = atan2(, a_2 + a_3 * C_3, a_3 * S_3) \quad \textbf{18}$$

$$\theta_2 = atan2(r, s) - \delta \quad \textbf{19}$$

2.3.2 Inverse Orientation

Having derived the values for the first 3 joints to satisfy the positional requirements, the last three can now be determined to satisfy the desired orientation. The desired final orientation, r, is shown in Equation 20, while the rotation caused by the first three joints, R_3^0, is shown in Equation 21, and the rotation due to the last three joints, R_6^3, is shown in Equation 22.

$$r = \begin{bmatrix} r_{1,1} & r_{1,2} & r_{1,3} \\ r_{2,1} & r_{2,2} & r_{2,3} \\ r_{3,1} & r_{3,2} & r_{3,3} \end{bmatrix} \quad \textbf{20}$$

$$R_3^0 = \begin{bmatrix} c_1 * c_{23} & s_1 & c_1 * s_{23} \\ s_1 * c_{23} & -c_1 & s_1 * s_{23} \\ s_{23} & 0 & -c_{23} \end{bmatrix} \quad \textbf{21}$$

$$R_6^3 = \begin{bmatrix} c_4 * c_5 * c_6 - s_4 * s_6 & c_4 * s_5 & c_6 * s_4 + c_4 * c_5 * s_6 \\ c_4 * s_6 + c_5 * c_6 * s_4 & s_4 * s_5 & c_5 * s_4 * s_6 - c_4 * c_6 \\ -c_6 * s_5 & c_5 & -s_5 * s_6 \end{bmatrix} \quad \textbf{22}$$

As shown in Equation 23, the final orientation in rotation matrix form is equal to the product of the rotation matrices from each of the joints. This can then be rewritten to Equation 24 to solve for the unknown joint angles. Keep in mind, the desired final orientation, r, and rotation due to the first three joints, R_3^0, are known at this point. Therefore, the right side of Equation 24 can be simplified using Equation 25.

$$r = R_3^0 * R_6^3 \quad \textbf{23}$$

$$R_6^3 = (R_3^0)^T * r \quad \textbf{24}$$

$$R = (R_3^0)^T * r = \begin{bmatrix} R_{1,1} & R_{1,2} & R_{1,3} \\ R_{2,1} & R_{2,2} & R_{2,3} \\ R_{3,1} & R_{3,2} & R_{3,3} \end{bmatrix} \quad \textbf{25}$$

Then, by combining Equations 22 and 25, the joint angles can be determined using the following equations:

$$R_6^3(3,2) = c_5 = R_{3,2} \quad \textbf{26}$$

$$\theta_5 = atan2(\pm\sqrt{1 - {R_{3,2}}^2}, R_{3,2}) \quad \textbf{27}$$

$$R_6^3(1,2) = c_4 * s_5 = R_{1,2} \quad \textbf{28}$$

$$R_6^3(2,2) = s_4 * s_5 = R_{2,2} \quad \textbf{29}$$

$$\theta_4 = atan2(R_{2,2}, R_{1,2}) \quad \textbf{30}$$

$$R_6^3(3,1) = -s_5 * c_6 = R_{3,1} \quad \textbf{31}$$

$$R_6^3(3,3) = -s_5 * s_6 = R_{3,3} \quad \textbf{32}$$

$$\theta_6 = atan2(R_{3,3}, R_{3,1}) \quad \textbf{33}$$

Equation 27 relies upon a trigonometric identity and that $\theta_5 \neq 0$. Furthermore, since there are two possibilities, the positive result was selected by default. With the determination of these joint angles, the inverse kinematics for this arm are complete. A desired position and orientation can now be specified and the joint angles required to reach that position can be determined. An example of the kinematics is shown below in Figure 2-7 and Figure 2-8. Desired joint angles of 10,20,30,40,50,60 were specified to determine the forward kinematics. The position and orientation from the forward kinematics were then used to verify the inverse kinematics.

```
>> [T JA Arm] = armKinematics(10,20,30,40,50,60,Arm);

Forward =

   -0.3344    0.9419   -0.0315    0.4804
   -0.9424   -0.3339    0.0200    0.0847
    0.0084    0.0364    0.9993    0.3448
         0         0         0    1.0000


Joint_Angles =

   10.0000   20.0000   30.0000   40.0000   50.0000   60.0000
```

Figure 2-7: Inverse Kinematics Code

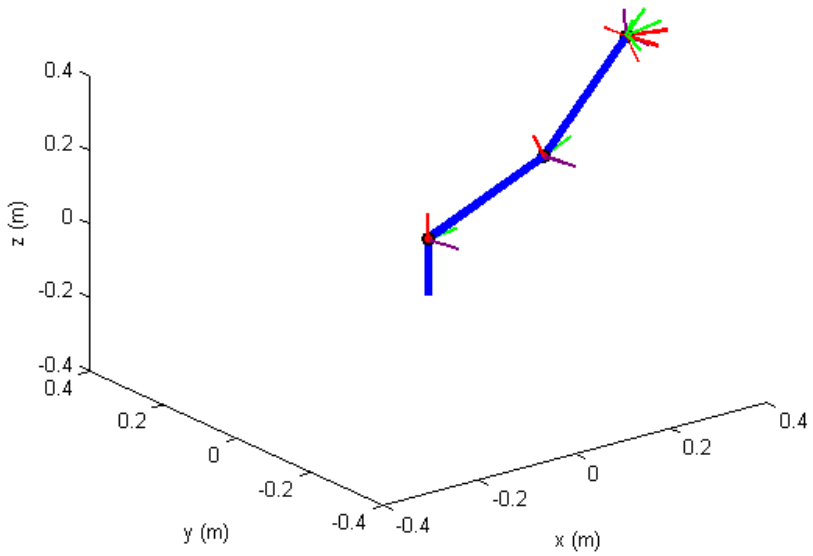

Figure 2-8: Inverse Kinematics Plot

As shown in the figures, the arm is in the anticipated geometric configuration and the joint angles match. The MATLAB used to calculate the inverse kinematics is shown in Appendix B: Inverse Kinematics.

2.4 Dynamics

The dynamics of the arm is an important subject to study. It allows one to determine the joint torques required based upon the position, velocity, and acceleration of the joints of the arm. Therefore, by determining the operating conditions of the arm the joint torques can be found and then used to determine the spring constants for the elastic elements and to correctly size the motors.

There are two main methods available to determine the dynamics of a system: Euler-Lagrange and Newton-Euler. Euler-Lagrange examines the total energy of the entire system, while Newton-Euler takes a more systematic approach by treating each link individually. While these two approaches are different and have their own pros and cons, in general they are considered equivalent and the choice between the two comes down to personal preference [41]. The Newton-Euler formulation will be used for this thesis and the following equations come from [42] which corrected several mistakes found it [41].

2.4.1 The Newton-Euler Formulation

The general approach to the Newton-Euler method is to start at the base and go up (forward recursion) the arm to the tip to determine the linear and angular motion, and then back down the arm (backward recursion) to calculate the forces and torques. The first step in this process begins with the dynamic model and both approaches rely upon the same general dynamic model shown in Equation 34.

$$M(q) * \ddot{q} + C(q, \dot{q}) * q + g(\dot{q}) = u \qquad \textbf{34}$$

where

q = Vector of joint variables

u = Vector of torques

M = Inertia matrix

C = Centrifugal and Coriolis terms

G = Gravity vector

Next, moving on to the Newton-Euler formulation the three relevant laws of mechanics are:

- Every action has an equal and opposite reaction
    - If link 1 applies force f and torque τ to link 2, then link 2 applies $-f$ and $-\tau$ to link 1
- The rate of change of the linear momentum is equal to the total force applied to the link
- The rate of change of the angular momentum is equal to the total torque applied to the link

Next, for a manipulator with n links, each link can be described by Figure 2-9.

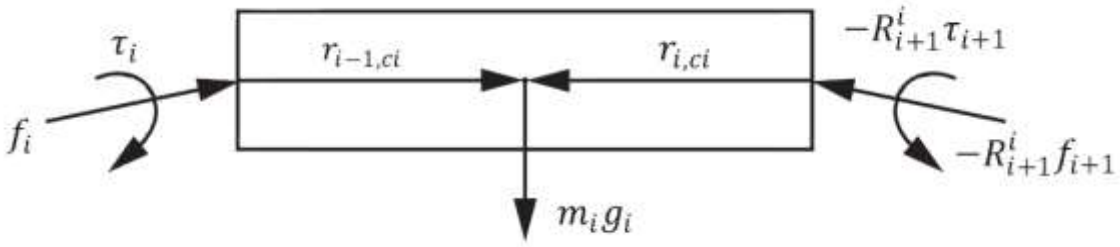

Figure 2-9: Forces and Torques on a Link [42]

The following definitions are also required to explain this figure and the following equations:

$a_{c,i}$ = Acceleration of the center of mass of link i
$a_{e,i}$ = Acceleration of the end of link i (origin of frame i+1)
ω_i = Angular velocity of frame i with respect to frame 0
α_i = Angular acceleration of frame i with respect to frame 0
z_i = Axis of actuation of frame i with respect to frame 0
g_i = Acceleration due to gravity
f_i = Force exerted by link i-1 on link i
τ_i = Torque exerted by link i-1 on link i
R^i_{i+1} = Rotation matrix from frame i to frame i+1
m_i = Mass of link i
I_i = Inertia tensor of link i about a frame parallel to frame i whose origin is at the center of mass of link i

$r_{i-1,ci} =$ Vector from the origin of frame i-1 to the center of mass of link i
$r_{i-1,i} =$ Vector from the origin of frame i-1 to the origin of frame i
$r_{i,ci} =$ Vector form the origin of frame i to the center of mass of link i

As shown from the above information, the forward kinematics are required to perform the dynamic simulation since rotation matrices and vectors relating joint positions must be known. Additionally, the masses, and inertias must also be known in addition to the information required for the kinematics.

2.4.1.1 Forward Recursion

The forward recursion is used to calculate the linear and angular motion of the arm. It begins at the base and moves up the arm to the tip. Given the previous information, the initial conditions:

$$\omega_0 = \alpha_0 = a_{c,0} = a_{e,0} = 0$$

and the knowledge that $z_0 = \begin{bmatrix} 0 \\ 0 \\ 1 \end{bmatrix}$, the forward recursion, where **i=1:n**, can be performed by solving Equations 37, 39, 40, and 41 in order and using Equation 36 to solve Equation 37.

$$z_i = R_i^0 * z_0 \quad \textbf{35}$$
$$b_i = (R_i^0)^T * R_{i-1}^0 * z_0 \quad \textbf{36}$$
$$\omega_i = (R_i^{i-1})^T * \omega_{i-1} + b_i * \dot{q}_i \quad \textbf{37}$$
$$\dot{\omega}_i = \dot{\omega}_{i-1} + z_{i-1}\ddot{q}_i + \omega_i \times b_i\dot{q}_i \quad \textbf{38}$$
$$a_i = (R_i^{i-1})^T * a_{i-1} + b_i * \ddot{q}_i + \omega_i \times b_i * \dot{q}_i \quad \textbf{39}$$
$$a_{e,i} = (R_i^{i-1})^T * a_{e,i-1} + \dot{\omega}_i \times r_{i-1,i} + \omega_i \times (\omega_i \times r_{i-1,i}) \quad \textbf{40}$$
$$a_{c,i} = (R_i^{i-1})^T * a_{e,i-1} + \dot{\omega}_i \times r_{i-1,ci} + \omega_i \times (\omega_i \times r_{i-1,ci}) \quad \textbf{41}$$

2.4.1.2 Backward Recursion

Next, the backward recursion, where **i=n:1**, can be performed to determine the joint forces and torques. This is done solving Equations **42** and **43** with the initial conditions:

$$f_{n+1} = f_0 \qquad \tau_{n+1} = \tau_0$$

Typically, $f_0 = \tau_0 = 0$, however, if force control is being used, then there is a desired force and/or torque at the tip.

$$f_i = R_{i+1}^i * f_{i+1} + m_i * a_{c,i} - m_i * g_i \quad \textbf{42}$$

$$\tau_i = R_{i+1}^i * \tau_{i+1} - f_i \times r_{i-1,ci} + \left(R_{i+1}^i * f_{i+1}\right) \times r_{i,ci} + \omega_i \times (I_i * \omega_i) + I_i * \alpha_i \quad \textbf{43}$$

2.4.2 Dynamic Simulation

Using the Newton-Euler based dynamic model, a dynamic simulation was performed to determine the torques on the individual joints. This information was later used to determine the appropriate springs and motors for the arm. This selection process will be covered in more detail in Chapter 3. The simulation was implemented in from scratch in MATLAB and then compared to results from Peter Corke's toolbox [43]. The MATLAB code is shown in Appendix C: Dynamics.

2.4.2.1 Parameter Specification

The first step in the dynamic simulation is determining the parameters. The important parameters are the length, mass, location of center of mass, and inertial tensors of each link. All of these were found from the SolidWorks model of the arm and can be found in Table 2-2. The information for the hand includes a 1 kg payload.

Table 2-2: Dynamic Parameters

Link	Length (m)	Mass (kg)	CGx (m)	CGy (m)	CGz (m)	Ixx (kg* m^2)	Iyy (kg* m^2)	Izz (kg* m^2)
Spinning Motor Assembly	0	3.34	0.00119	-0.08468	-0.00167	0.00722	0.00804	0.01099
Lower Arm	0.304	1.55	-0.16192	0.01293	0	0.00197	0.01378	0.01424
Elbow	0.021	0.45	0.008769	0.000223	0.056031	0.000209	0.000782	0.000795
Spinning Forearm	0.314	1.65	0	0.96270	0	0.00253	0.00701	0.00729
Wrist	0	0	0	0	0	0	0	0
Hand	0	1.15	0.06645	0	0.00130	0.00014	0.00041	0.00049

In addition to the parameters for the arm, $\hat{q}$, the vector joint variables must be determined, where $\hat{q} = \begin{bmatrix} q \\ \dot{q} \\ \ddot{q} \end{bmatrix}$ and q is the vector of joint angles, $\dot{q}$, the vector of angular velocities, and $\ddot{q}$, the vector of angular accelerations. These values were created by generating a trajectory for each joint to follow. The trajectories were created by specifying a starting angle, an amount to move, and an average velocity. The start position was specified such that the trajectory would result in the highest torques on the arm (ex: having the arm horizontal instead of vertical). The start position resulting in the greatest torques due to a combination of the motion and gravity was selected. An average joint speed was determined experimentally based upon human movement. This was done by timing how long it took to move each corresponding joint. Table 2-3 shows the start angle, end angle, and time for each joint.

Table 2-3: Vector Joint Variable Formulation

Joint	Start Angle (qz) (rad)	Angle to Move (qr) (rad)	Average Velocity (rad/s)
1	0	$\frac{\pi}{2}$	$\frac{\pi}{2}$
2	0	$\frac{\pi}{2}$	$\frac{\pi}{2}$
3	$\frac{-\pi}{8}$	$\frac{\pi}{2}$	π
4	0	$\frac{\pi}{2}$	$\frac{\pi}{2}$
5	0	$\frac{\pi}{2}$	π
6	0	$\frac{\pi}{2}$	π

Joints having parallel z axes were tested at the same time. Therefore, three different movements were tested. This was done to generate the maximum dynamic loads based upon the specified 1 kg payload, start and end locations, and average velocities previously discussed. The first test examined joints 2, 3, and 5. q_z, the start angle vector for this test, and q_r, the angular distance to move, are shown below:

$$q_z = \begin{bmatrix} 0 \\ 0 \\ \frac{-\pi}{8} \\ 0 \\ 0 \\ 0 \end{bmatrix} \qquad q_r = \begin{bmatrix} 0 \\ \frac{\pi}{2} \\ \frac{\pi}{2} \\ 0 \\ \frac{\pi}{2} \\ 0 \end{bmatrix}$$

This resulted in the trajectories shown in Figure 2-10. Note that the velocity and acceleration for joints 3 and 5 are the same and therefore overlap. It also resulted in the plot of joint torques shown in Figure 2-11.

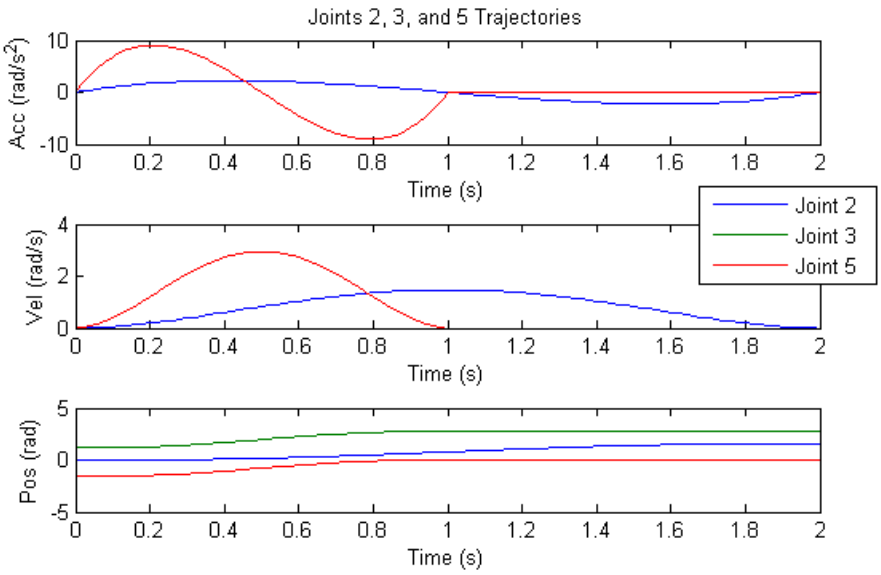

Figure 2-10: Joints 2, 3, and 5 Trajectories

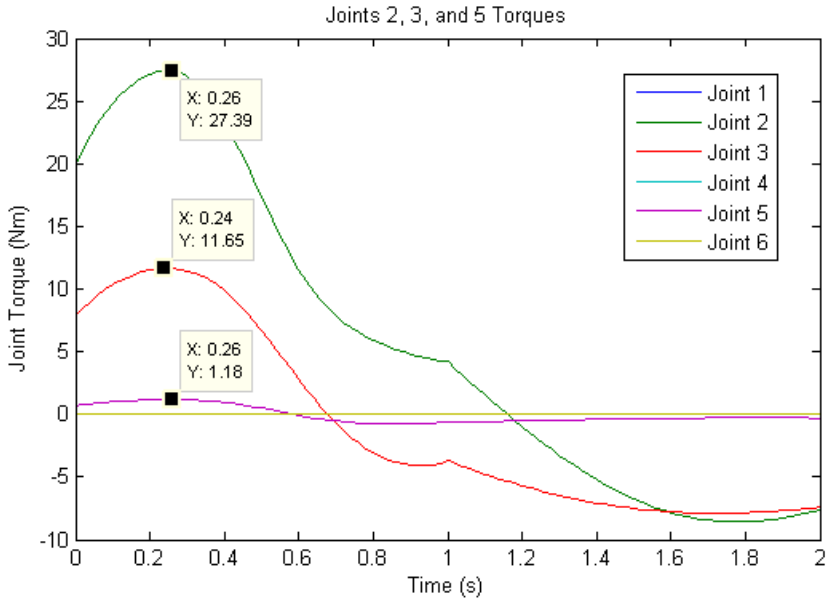

Figure 2-11: Joints 2, 3, and 5 Torques

As shown in Figure 2-11, the maximum torque is 27.39 Nm for joint 2, 11.65 Nm for joint 3, and 1.18 Nm for joint 5.

Next, joints 1 and 6 were tested with the following q_z and q_r:

$$q_z = \begin{bmatrix} 0 \\ 0 \\ 0 \\ 0 \\ 0 \\ 0 \end{bmatrix} \qquad q_r = \begin{bmatrix} \frac{\pi}{2} \\ 0 \\ 0 \\ 0 \\ 0 \\ \frac{\pi}{2} \end{bmatrix}$$

which resulted in the trajectories shown in Figure 2-12 and the torques shown in

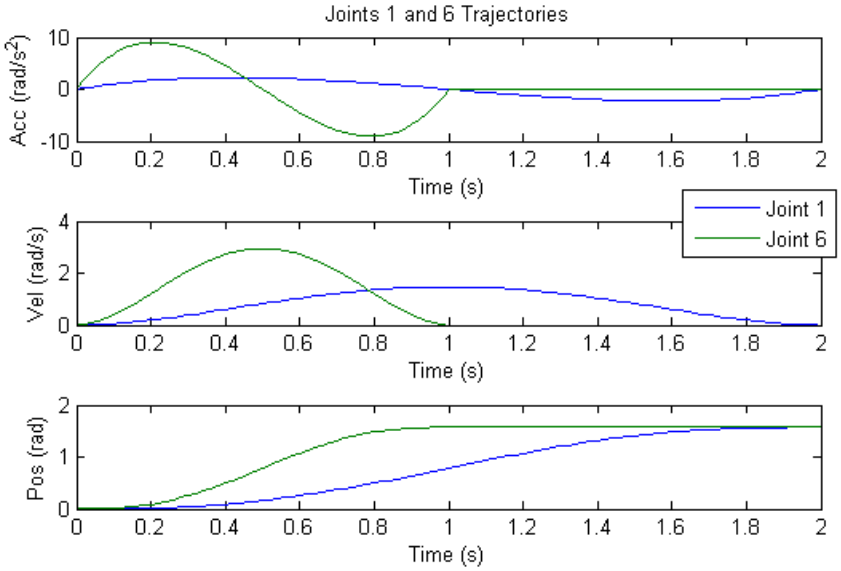

Figure 2-12: Joints 1 and 6 Trajectories

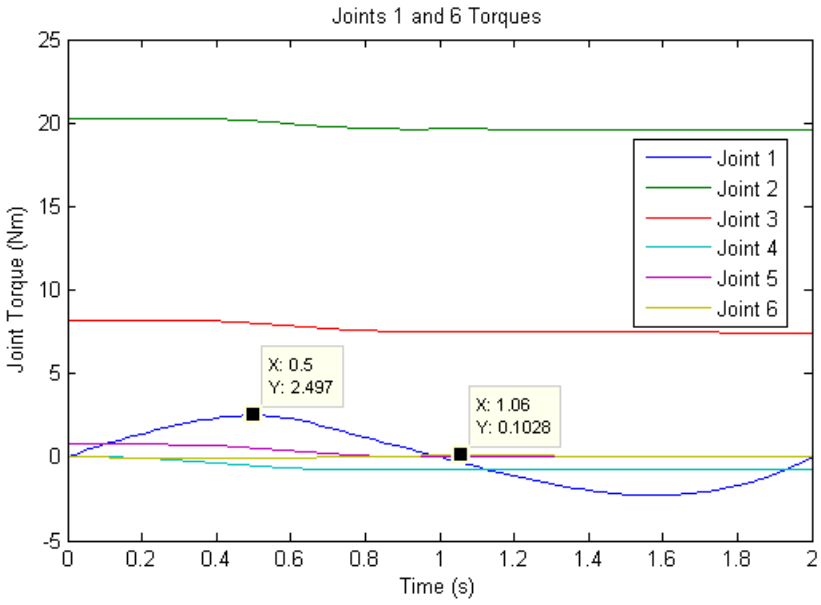

Figure 2-13: Joints 1 and 6 Torques

The maximum torque for joint 1 is 2.5 Nm while the maximum torque for joint 6 in this configuration is 0.1 Nm, however, since joints 5 and 6 share an origin, rotating joint 6 by $\frac{\pi}{2}$ radians would result in the same torque as joint 5. Therefore, the maximum torque for joint 6 is actually 1.18 Nm.

Lastly, joint 4 was tested with the q_z and q_r shown below:

$$q_z = \begin{bmatrix} 0 \\ 0 \\ 0 \\ 0 \\ \frac{\pi}{2} \\ 0 \end{bmatrix} \qquad q_r = \begin{bmatrix} 0 \\ 0 \\ 0 \\ \frac{\pi}{2} \\ 0 \\ 0 \end{bmatrix}$$

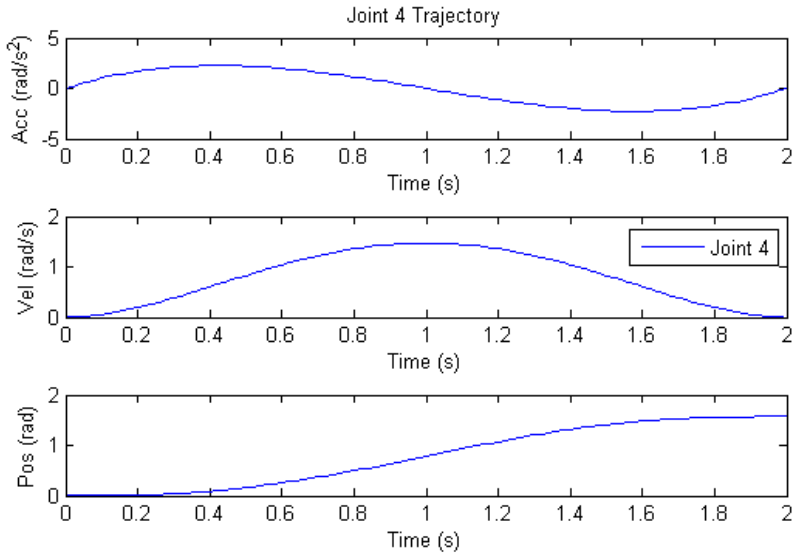

Figure 2-14: Joint 4 Trajectory

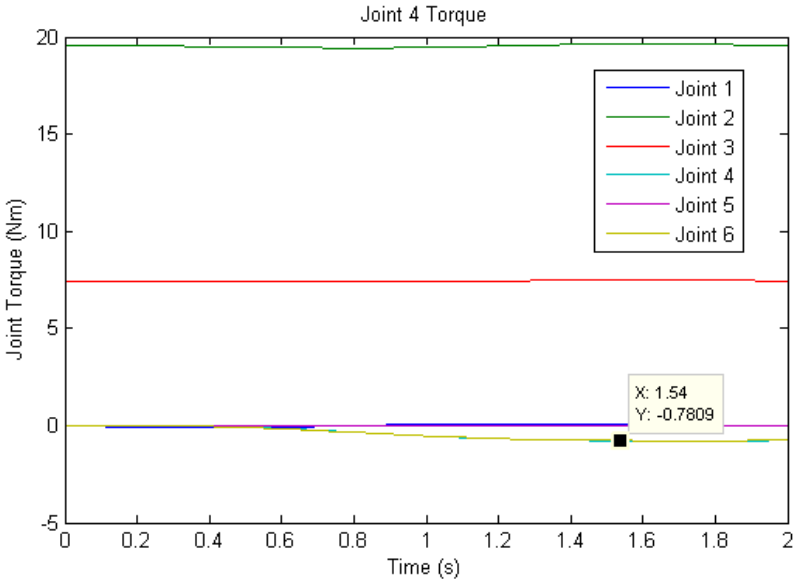

Figure 2-15: Joint 4 Torque

The test for joint 4 required rotating joint 5 by $\frac{\pi}{2}$ so that the lever arm for the load in the hand was largest. This resulted in a maximum torque of 0.78 Nm. A summary of the maximum torques is shown in Table 2-4.

Table 2-4: Joint Torques

Joint	Torque (Nm)
1	2.5
2	27.4
3	11.65
4	0.7
5	1.18
6	1.18

The maximum torques shown in Table 2-4 and found using the dynamic simulation can be used to determine the necessary springs and motors as will be discussed in the next chapter.

Chapter 3: System Design

This chapter covers the mechanical design and describes the high-level electrical architecture of a compliant robotic arm containing tactile sensors. First the design requirements which the system must conform to are covered. Next, the mechanical design is discussed in detail including the process used to select the springs and motors and component design and analysis. After, the design of the tactile sensor shell is covered and finally the high level electrical structure is discussed.

3.1 Design Requirements

The first step in developing the design was to identify a list of design requirements which the robotic arm must conform to. These constraints included:

- Arm must be capable of manipulating a 1 kg payload
- Arm is approximately the size of a small human
- Arm is adequately covered in tactile sensors
- Arm must have six degrees of freedom split into a 3 DOF arm and 3 DOF wrist
- Each joint must have series elastic actuators which are easily assembled
- No joint will deflect more than 5 degrees at maximum dynamic loads
- Each joint can deflect 15-20 degrees in either direction
- Arm can be easily integrated with a robotic hand

The purpose of this arm is to research sensitive manipulation techniques for a humanoid platform, hence the requirement of approximating the size of a small human. Additionally, despite the fact that it is human sized, the arm has a much smaller payload that a human arm is capable of handling. This is because it is actually very difficult to replicate the power density of muscle [3]. Additionally since the purpose of the arm is research instead of commercially focused, a 1 kg payload is more than sufficient.

Again, since the purpose of this arm is to develop new approaches to sensitive manipulation, it must be adequately covered in tactile sensor. However, this thesis is focused on the construction of the arm as a platform and therefore a partial tactile shell has been constructed but the tactile sensor coverage has not been optimized. This being said, the mechanical design was performed keeping the shell in mind as will be mentioned later in this chapter.

The arm must also have six degrees of freedom which replicate those of a human arm. Therefore, they must be split into a 3 DOF arm and a 3 DOF wrist. More specifically, the 3 DOF arm must include a 2 DOF shoulder and a 1 DOF elbow with an asymmetric joint range. Additionally, the wrist must include one twisting and two pivoting motions. As was seen when deriving the inverse kinematics, this configuration also simplified the kinematics of the arm. While the arm itself must have 6 degrees of freedom, this thesis only focuses on the first 4 DOF. This was done to aid in satisfying the requirement of being easily integrated with a hand.

Lastly, every joint must contain series elastic actuators. The benefits of series elastic actuators have already been highlighted earlier in section 1.1.2 with the overall goal being to introduce compliance into the arm. There is also a sub-requirement to develop a self-contained series elastic module which can be assembled outside of the robot. Finally, to avoid excessive compliance, there is a requirement that no joint deflects more than 5 degrees due to dynamic loading. Additionally, the joint should have enough travel to deflect a total of 15 to 20 degrees in either direction. These two requirements will be used to determine the springs for the series elastic actuators.

The success of this arm will be gauged on the meeting of these design requirements. Additionally, the mechanical design, electrical design, and software architecture were constructed to meet these requirements. Lastly, the system evaluation was performed such that each of these requirements is thoroughly tested.

3.2 Mechanical Design

While many aspects were considered for the mechanical design, such as weight, aesthetics, size, and range of motion; the primary emphasis of the mechanical design was on the series elastic actuators. This can be split into the selection of the springs and motors, the design of the SEA modules and joints, and the cable routing for the arm. Additionally, the design of the base is discussed in this section along with the design of the shell for the tactile sensors.

3.2.1 Spring and Motor Selection

The process used for the spring and motor selection received a significant amount of attention on this project. The first step is developing a good dynamic model to calculate the required joint torques as described in Section 2.4.

The joint torques were then converted into forces on the springs and torques on the motor which were used for the selection. The first step is to convert the joint torque, τ_{joint}, into a force, F_{cable}, which represents the tension in the cable using r_{joint}, the length of the lever arm at the joint termination location, as shown in Equation 44.

$$F_{cable} = \frac{\tau_{joint}}{r_{joint}} \quad \textbf{44}$$

This force can then be used to determine the motor torque, τ_{motor}, using the radius of the motor pulley, r_{motor}, as shown in Equation 45. Using the torque and the maximum velocities specified when generating the trajectories, motors can be selected.

$$\tau_{motor} = F_{cable} * r_{motor} \quad \textbf{45}$$

The motor requirements and the motor specifications are shown in

Table 3-1.

Table 3-1: Motor Specifications

Joint	Required		Actual	
	Torque (Nm)	Speed (rpm)	Torque (Nm)	Speed (rpm)
1	2.0	19	4.6	59
2	1.5	289	3.0	300
3	2.6	125	5.3	127
4	0.6	38	2.3	35

The smallest possible motor and gearbox were selected which could produce the required torque. Once a size was determined, the most powerful gearbox and motor combination still capable of generating the necessary speed were selected. It can also be seen that the motor torque is different from the joint torque because of the gear ratio due to the joint lever arm and motor pulley radius. Therefore, the motor selection process was an iterative one which happened concurrently with the mechanical design. Both the motor requirements and mechanical design iterated several times before the motor and pulley sizes were finalized.

The motors for this project, all provided by Maxon Motors, were selected primarily due to time constraints and it is possible that smaller motors can be selected to perform at the same levels. All of the joints are powered by brushed motors except for the shoulder rotation (Joint 1) which has a brushless motor. The relevant specifications for each of the motors and gearboxes are shown in

Table 3-2 and the work performed to select the motors is shown in Appendix D.

Table 3-2: Motor and Gearbox Specifications

Joint	Motor Diameter (mm)	Motor Torque (mNm)	Motor Speed (rpm)	Motor Efficiency (%)	Motor Power (W)	Motor Voltage (V)	Gearbox Diameter (mm)	Gearbox Ratio	Gearbox Efficiency (%)
1	30	60.7	9340	81	60	24	32	111:1	70
2	40	170	7580	91	150	24	42	26:1	81
3	40	170	7580	91	150	24	42	43:1	72
4	22	15.3	18000	84	20	24	22	260:1	74

Additional steps are required to calculate the spring force due to the configuration of the springs. Since there are two half compressed springs which counterbalance each other, the effective spring rate is more complex. This changes the equation for the spring force as shown in the equations below. It starts with the general equation for a spring (Equation 46) and ends with the equation for the effective spring rate (Equation 52). Equation 48 is the most significant equation as it is where having two springs is introduced. The equation is structured such that the resting location for both springs, x_0, is at half of the total length of the spring, L, as shown by Equation 49. Additionally, Equation 48 has the two springs working in opposite directions.

$$F = k * \Delta x \quad \textbf{46}$$

$$F = k * (x_0 + \Delta x) - k * (L - (x_0 + \Delta x)) \quad \textbf{47}$$

$$F = k * x_0 + k * \Delta x - k * L + k * x_0 + k * \Delta x \quad \textbf{48}$$

$$x_0 = \frac{L}{2} \quad \textbf{49}$$

$$F = 2 * k * \frac{L}{2} - k * L + 2 * k * \Delta x \quad \textbf{50}$$

$$F = 2 * k * \Delta x \quad \textbf{51}$$

$$k = \frac{F}{2 * \Delta x} \quad \textbf{52}$$

As shown in Equation 52, the effect of having the two counter balancing springs is that the spring force is half of what is required with a single spring. This is expected given that it is two springs in parallel and is beneficial as it practically means that smaller springs can be used. However, having the two half compressed springs ultimately results in needing to have double the travel as shown below.

Given the requirement that the arm should not deflect more than 5 degrees under dynamic load, the amount of deflection Δx, can be calculated using Equation 53, where c_{joint} is the circumference of the pulley at the joint.

$$\Delta x = c_{joint} * \frac{5}{360} \quad \textbf{53}$$

However, this is the amount of travel in only one direction. Since the spring must move this distance in both directions, the total amount of travel the spring must be capable of is double this as shown in Equation 55.

$$x = 2\Delta x \quad \textbf{54}$$

$$x = 2 * c_{joint} * \frac{5}{360} \quad \textbf{55}$$

Substituting Equations 44 and 53 into Equation 52 results in the necessary spring rate for the joint as shown in Equation 56. Additionally, joints 2, 3, and 4 have two springs on either side instead of one. This decision will be explained in later sections but the effect is that the spring rate is further cut in half resulting in Equation 57.

$$k = \frac{F_{cable}}{2 * \Delta x} \quad (56)$$

$$k = \frac{F_{cable}}{4 * \Delta x} \quad (57)$$

A suitable spring can selected now that the spring rate (k) and total amount of travel (x) are known. However, the inside and outside diameters are also relevant parameters but are dictated by the mechanical design instead of the dynamics. A summary of the spring requirements and the specifications of the selected springs are shown in Table 3-3.

Table 3-3: Spring Specifications

Joint	Required		Actual				Spring (leespring.com)
	Spring Constant (N/mm)	Compressible Distance (mm)	Spring Constant (N/mm)	Compressible Distance (mm)	Hole Diameter (mm)	Free Length (mm)	
1	47.63	12.88-17.17	46.63	13	15.88	38.1	LHL 625C 03
2	49.74	4-5.31	51.84	9.65	15.88	31.75	LHL 625C 02
3	47.63	7.49-10	51.84	9.65	15.88	31.75	LHL 625C 02
4	22.24	6.66-8.87	23.47	7.39	15.24	8.64	LWM15 080 0864s

The springs were purchased from Lee Spring. As shown in Table 3-3, all of the springs can fit in a 15.88 mm hole. Additionally, the shoulder and elbow pivot joints were configured so that they used the same springs. Furthermore, all of the joints use four springs except for the shoulder rotation joint which uses two. The springs for the wrist rotation joint have a much shorter free length because they are wave springs instead of die springs. Ideally wave springs would have been used for all of the joints because of this decrease in free length; however, the spring constants do not go high enough while maintaining an acceptable diameter. Lastly, all of the springs were selected to have the same or a

higher spring force. The increased spring forces have little effect on the deflection at maximum dynamic load as all of the joints deflect more than 4 degrees but less than 5. Also, keep in mind that these calculations were all performed with a 1 kg load. Therefore, the system will be stiffer when moving without a payload. The work performed to determine the springs is shown in Appendix D.

3.2.2 Joints and Series Elastic Modules

A heavy emphasis was placed on developing standalone modules for the spring systems. This was partially due the problem with tensioning the system experienced in [11], but mostly because one of the primary outcomes of this project is a compact series elastic module. Each joint utilizes a different method for implementing the SEA; however, the shoulder and elbow pivots are very similar. The shoulder rotation joint is the least modular solution and follows an approach similar to that in [11]. Lastly, the wrist rotation joint utilizes what may be the most significant approach which can be integrated anywhere in the system and act like traditional cable/chain tensioners.

3.2.2.1 Shoulder Rotation Joint

The first joint is the shoulder rotation joint which also happens to use the simplest form of SEA in the arm. It uses a SEA integration similar to that developed in [11]. The difference is that this configuration will use a bolt to compress one of the springs completely instead of using a pin as was done in [11].

The SEA requires several idler pulleys as the cable changes planes multiple times. As shown in Figure 3-1, the cable terminates in a stopper which is housed in a plunger which then compresses the spring. One of the unique aspects of this design is that the forces generated by having the springs at half compression result in a tension throughout the cable. The downside of this is that the average force on the components is increased; however, one of the benefits is that a separate cable tensioning system is

not required. The figure also shows that there is a linear potentiometer which measures the movement of the plunger. The potentiometer uses a magnet and therefore a small screw attached to the plunger is used to move the magnet.

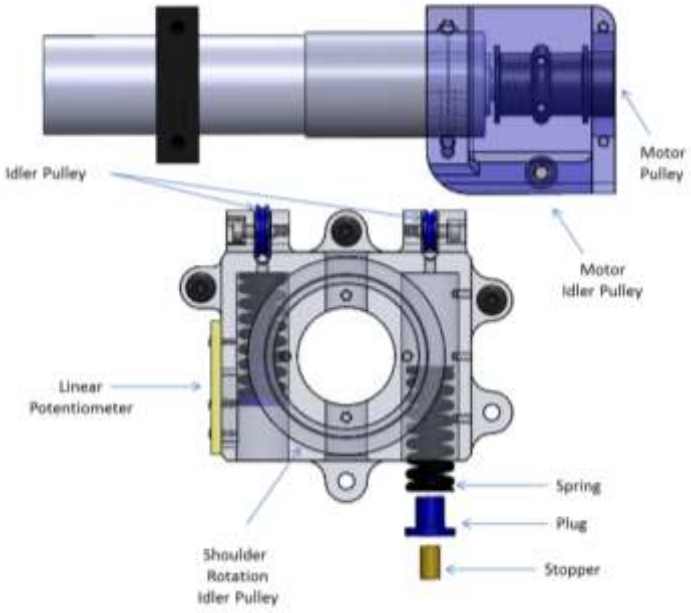

Figure 3-1: Shoulder Rotation Joint SEA

While the cables are omitted from Figure 3-1, they are shown from one angle in Figure 3-2. The cable routing for this joint is the most complicated to visualize. One direction is shown with a solid line while the other with a dashed line. The solid cable going from the motor idler pulley to the shoulder rotation idler pulley has been shifted down from its actual position to improve clarity of the figure. As shown in Figure 3-2, the two idler pulleys are different diameters. This is so that the cables will be offset and do not interfere. The pulleys then had to be offset so that both cables still entered the center of the spring.

Moving from the spring, over these idler pulleys, the cable then changes planes and passes over the shoulder rotation idler pulley which is concentric with the joint but is free to rotate about the joint.

From this idler pulley the cable moves around the motor idler pulley where it again changes planes and is attached to the motor.

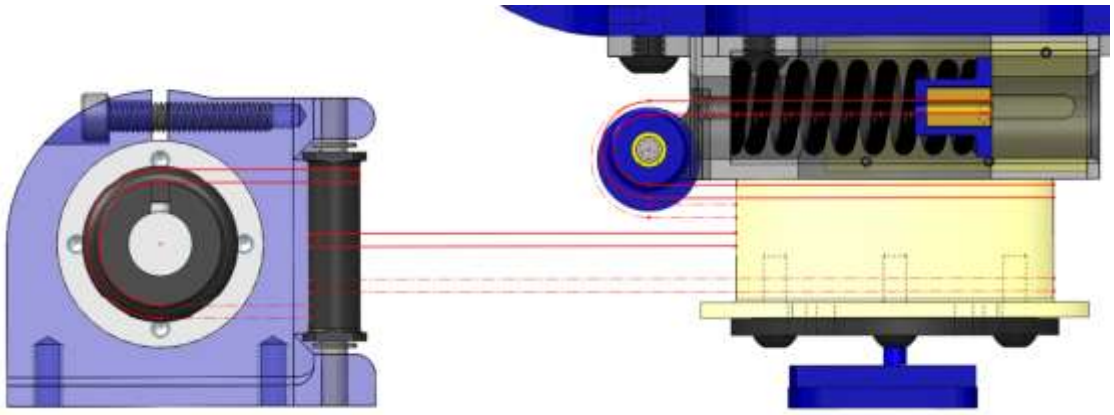

Figure 3-2: Shoulder Rotation Joint Cable Routing

This joint, like the other three, uses two separate cables. The process for cabling the joint is to terminate both of these cables inside of the spring. Then, two bolts are used to compress both of these springs. One spring is fully compressed while the other is only partially compressed. The first is fully compressed so that each spring ends up being half compressed while the second is only partially compressed to take up the added slack created when terminating the cables on the motor. The cables are then routed as previously described and then terminated on the motor. The bolts are then removed and they system is at the steady state location with each spring at half compression.

3.2.2.2 Shoulder Pivot Joint

The shoulder pivot joint is the next joint in the kinematic chain. It and the wrist rotation joint have the innovative implementations of series elastic actuators. In this case, it is not the SEA itself which is innovative, but the location of the SEA.

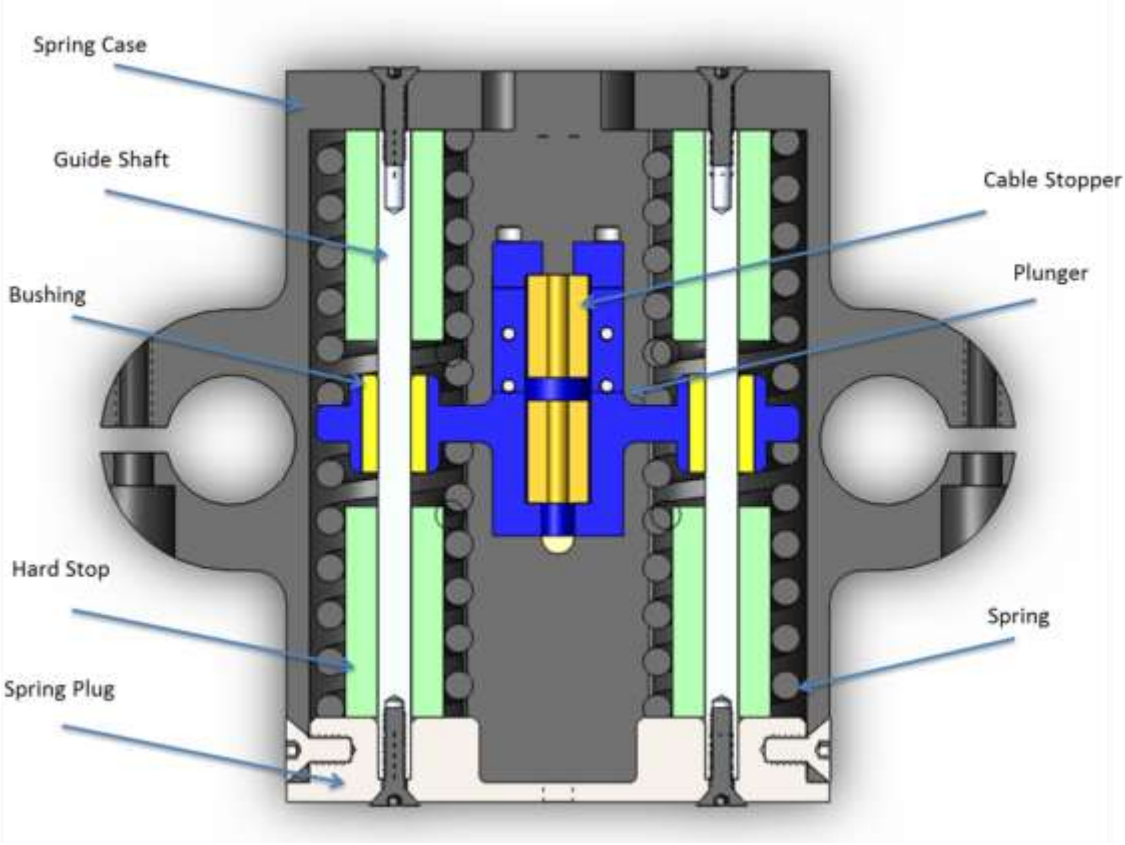

Figure 3-3: Shoulder Pivot Joint SEA

This module is used for both the shoulder pivot joint and the elbow with only the attachment method differing. Furthermore, the concept behind this module is also used for the wrist rotation joint, however the attachment to the cable is different. As shown in Figure 3-3, the elastic module is composed of several different parts. It has four springs all of which push against the spring case/spring plug and the plunger. The plunger is attached to the cables and moves to compress the springs. It slides along the guide shaft, but the motion is limited by the hard stops. Like the previous joint, there are still cable stoppers which attach to the cable and are held by the plunger.

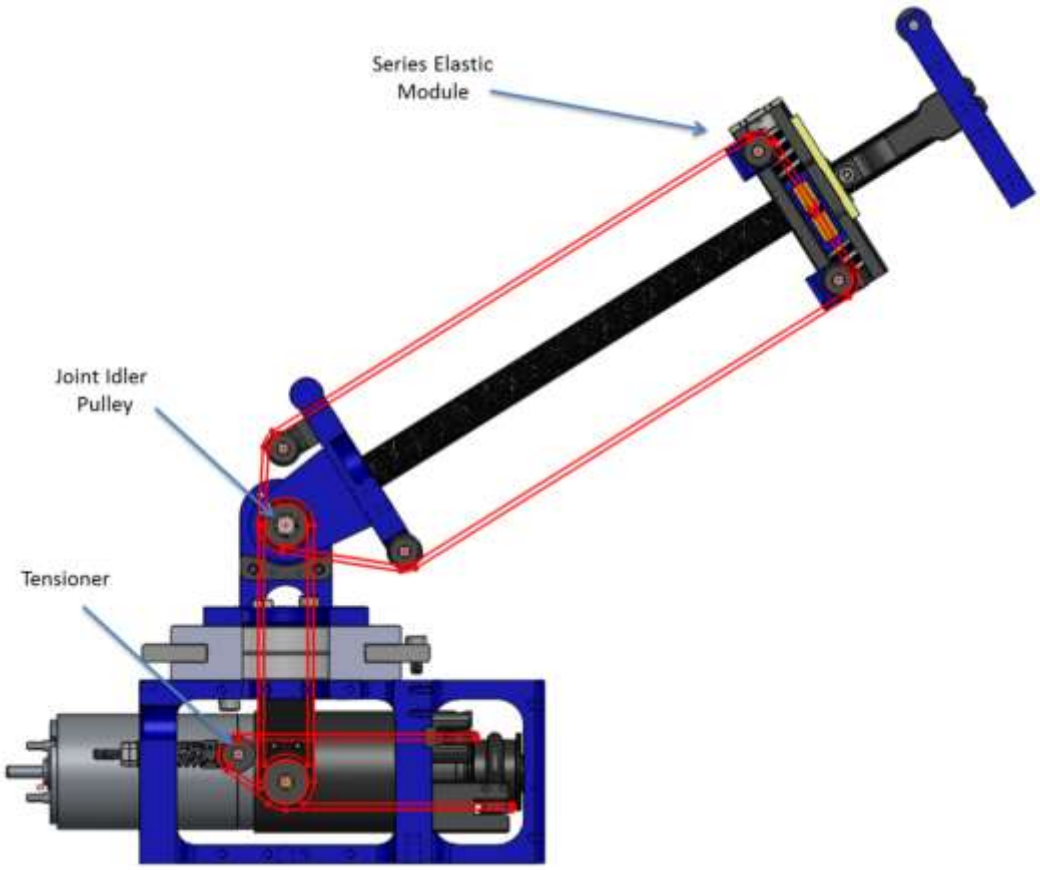

Figure 3-4: Shoulder Pivot Joint Cable Routing

The cable routing for this joint is shown in Figure 3-4. As shown, the motor has been located low in the base to lower the center of gravity and to reduce the mass of the arm thereby reducing the torque required. Additionally, the figure shows that this configuration requires a tensioner as all of the forces holding the springs at half compression are now contained within the module. Additionally there must be an idler pulley at the point of rotation for the joint but then the cables can be terminated.

The process for physically routing and tensioning the cable begins by routing a cable through one of the termination points on the motor pulley and then wrapping it around this pulley several times. The cable was then routed along the path shown in Figure 3-4 back through the other termination point on the motor pulley. The series elastic module was slid down the arm from the position shown in Figure 3-4. Excess cable was left to aid in terminating the cable in the spring plunger. The cable was then cut

in the middle of the spring plunger and terminated using the two cable stoppers shown in Figure 3-3. Locktite 680 was used on the dyneema between the brass cone and brass cable stopper. The arm was then moved to one extreme, the cable pulled tight, and terminated on the motor pulley using the same brass cone and Locktite 680. It was then moved to the other extreme, terminated at an appropriate length, and then had the Locktite 680 applied. The length was determined by terminating the cable but not applying Locktite and pulling the series elastic module into position. The cable length was set so that the module was kept as far from its final location as possible while still having bolts reach it. Once all four locations were terminated, the module was brought to its final position using the bolts and the tensioner was fully tightened resulting in a completely tensioned system.

In fact, this choice allows for the ability to significantly reduce the torque required by the motor for this joint. As shown in Figure 3-5, by strategically locating the series elastic module at the end of the link instead of directly at the joint as was done in the elbow, the lever arm is much larger. As such the torque required by the motor is greatly reduced. This is very beneficial because the lower link also requires the most joint torque and by doing this the torque is actually brought below the amount required for the elbow joint.

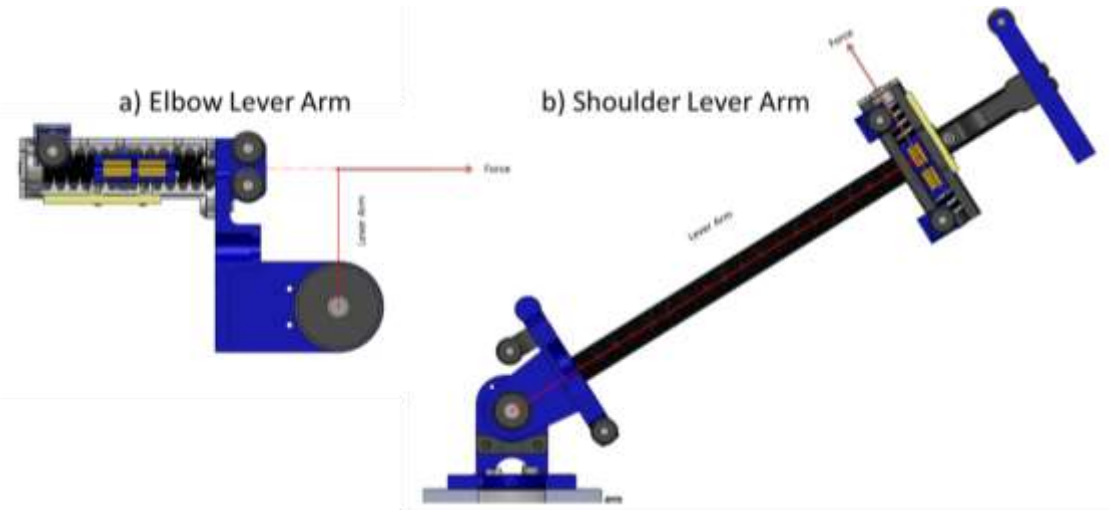

Figure 3-5: Joint Lever Arms

3.2.2.3 Elbow Pivot Joint

Next, the elbow pivot joint is very similar to the shoulder pivot joint. It uses the same series elastic module as the shoulder rotation joint, but has a different housing to allow for integration into the joint. Figure 3-6 shows this joint in the three primary positions. Figure 3-6a shows the plunger in the fully compressed up position, Figure 3-6b shows it in the steady state or half compressed position, and Figure 3-6c shows it in the fully compressed down configuration.

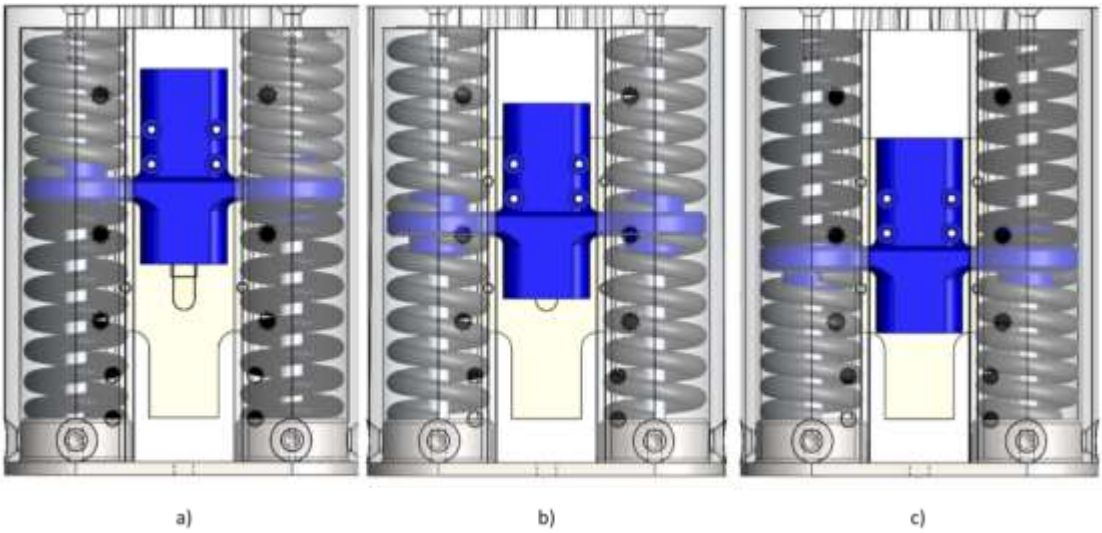

Figure 3-6: Elbow Pivot Joint SEA

Ideally, the lever arm for this joint would also have been extended, but this could not be accomplished because the wrist rotation joint directly follows this joint. However, steps were taken to maximize the length of the lever arm. Remember that one of the requirements of this project is to develop a robotic arm which replicates the joints of a human. The human elbow is very asymmetric and can bend much more in one direction than the other. To replicate this, the pivot for this joint was offset from the center. This had the added benefit that the lever arm for the series elastic element was also extended.

The cabling for this joint is shown in Figure 3-7. As shown in the figure, the motor for this joint is also located in the base for the same reasons listed for the shoulder pivot joint. This does have one down side that the position of this joint is coupled to the position of the shoulder pivot joint. This is because the cable must wrap around an idler pulley concentric with the shoulder pivot joint. Therefore, as the shoulder pivot joint moves, the length of the cable for either side of the joint will change. Luckily, this problem will automatically be fixed by the controller for this joint. Because the controller has position control for the joint, it will sense this change in position with the rotary potentiometer and adjust the motor position accordingly. There will, however, be minor movements required by the motor as the shoulder pivot joint is moved. As the shoulder pivot joint moves, the motor for the elbow pivot joint will have to move at the same speed to maintain the relative position of the elbow pivot joint.

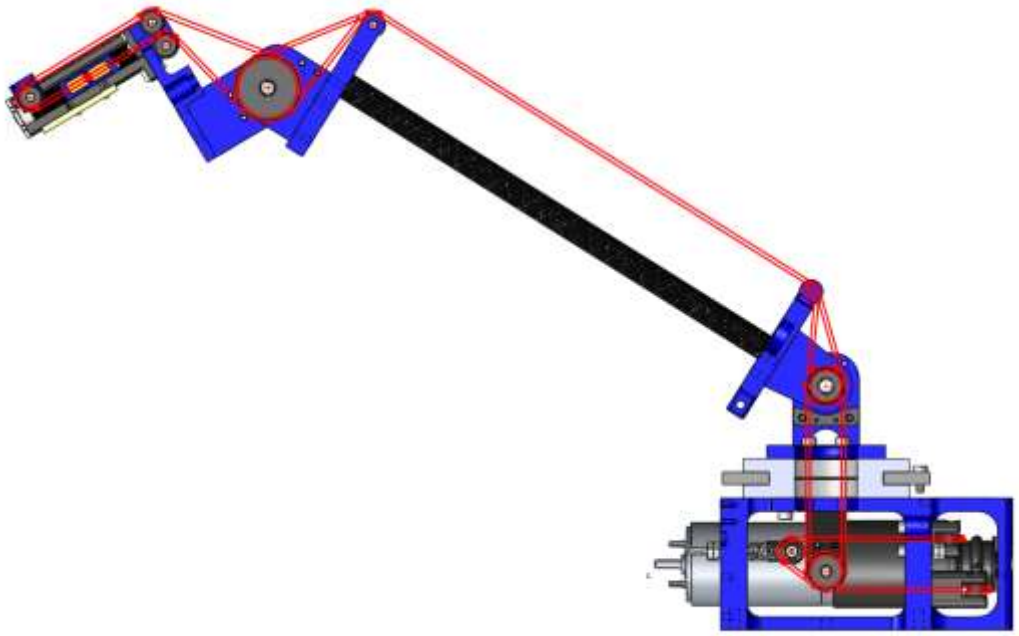

Figure 3-7: Elbow Pivot Joint Cable Routing

As shown in Figure 3-7, the idler pulley at the elbow pivot joint is much larger than the idler pulley at the shoulder pivot joint. This was actually a strategic decision made to increase the amount of

deflection on the spring since the deflection is directly related to the circumference. This was done so that the two joints could use the same springs. However, this joint has a much larger travel than the shoulder pivot joint. As such, Figure 3-3 and Figure 3-6 show that there is no hard stop for the elbow pivot joint spring assembly. This is because the spring bottoms out at approximately 20 degrees of deflection.

Lastly, as shown in Figure 3-7, the cables for this joint are both on the top of the lower link. This was done both to leave clear space to put electronics, but more importantly to allow for the asymmetrical movement of the elbow. If one of the cables had been on the top while the other was one the bottom, then the bottom cable would have limited the movement of the elbow joint.

The process for routing and tensioning the cable is nearly identical to that used for the shoulder pivot joint. The difference is that the series elastic module for this joint cannot be moved. Therefore, the idler pulley at the tip of the spring box is removed during the initial cabling process and then replaced just before tightening the tensioner.

3.2.2.4 Wrist Rotation Joint

The final joint of this arm is the wrist rotation joint. It also contains the most innovative form of series elastic actuators which has not been seen before and therefore is one of the more significant contributions of this work. The implementation can best be considered as a series elastic actuator implemented as a traditional cable tensioner such as those found in a car. This actuator is smaller than the other two series elastic modules and utilizes wave springs instead of traditional compression springs. This mechanism is shown in Figure 3-8.

As shown in the figure, there is no termination of the cable on the series elastic element. Instead, there are two idler pulleys located on the plunger. Therefore, if there is a force applied by

either the motor or externally on the arm, it pulls the plunger closer to the external idler pulley. This effectively works the same as a traditional series elastic actuator but no longer has to be located at the motor or joint as has been traditionally required by cable driven series elastic actuators.

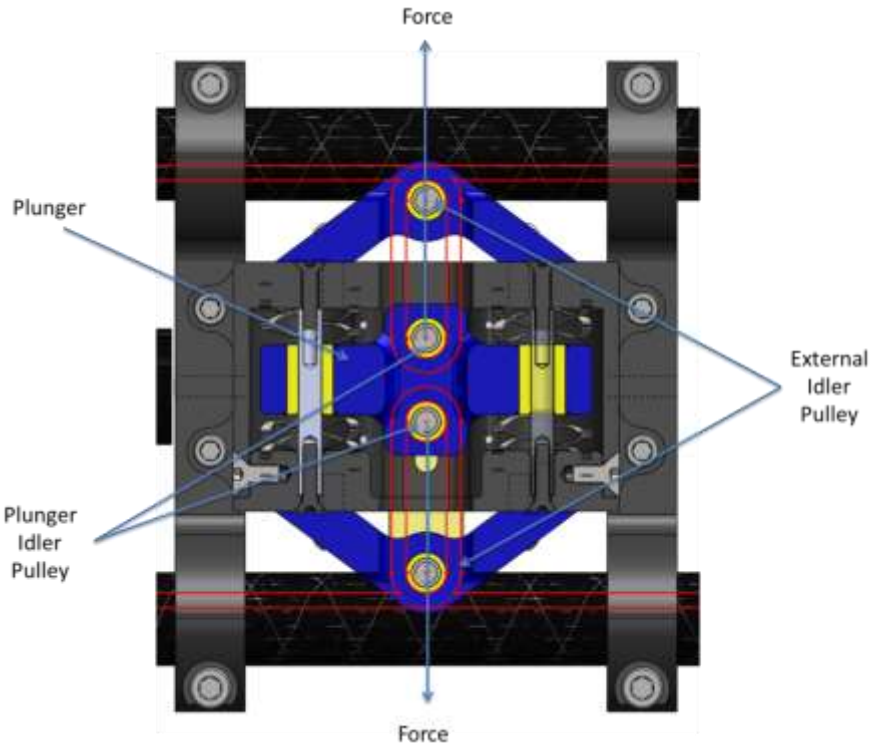

Figure 3-8: Wrist Rotation Joint SEA

One down-side of this approach, at least for this instance, is that it decreases the spring deflection by a factor of two. Therefore, for this form of SEA, Equation 53 must be modified to Equation 58 shown below. This is due to the fact that the cable wraps around the plunger idler pulley. Therefore if the plunger idler pulley moves a distance of 1, each side of the cable moves a distance of 1 resulting in a total cable distance change of 2.

$$\Delta x = \frac{c_{joint}}{2} * \frac{5}{360} \quad \textbf{58}$$

It is also important to notice that the movement of both sides of the cable is coupled since the plunger idler pulleys are attached to the same plunger. Therefore, if slack is created on one side, it is taken up on the other and therefore the total length of the cable does not change.

The last important aspect of this version of a series elastic actuator is that the cable wraps 180 degrees around the plunger idler pulley. As such the relationship between the movement of the plunger and the change in cable length is perfectly linear. This is one of the aspects which distinguishes this approach from normal cable tensioning systems. Traditional cable tensioning systems have a spring lever arm which rotates to take up any slack in the system. As such there is not a linear relationship between the deflection of the spring and the change in length of the cable since the angle must be taken into account. The other significant attribute is that the deflection of the spring is being measured since it is a series elastic actuator whereas traditional cable tensioning systems have no regard for the position. Like the other series elastic modules, this configuration requires a separate cable tensioner as shown in Figure 3-9.

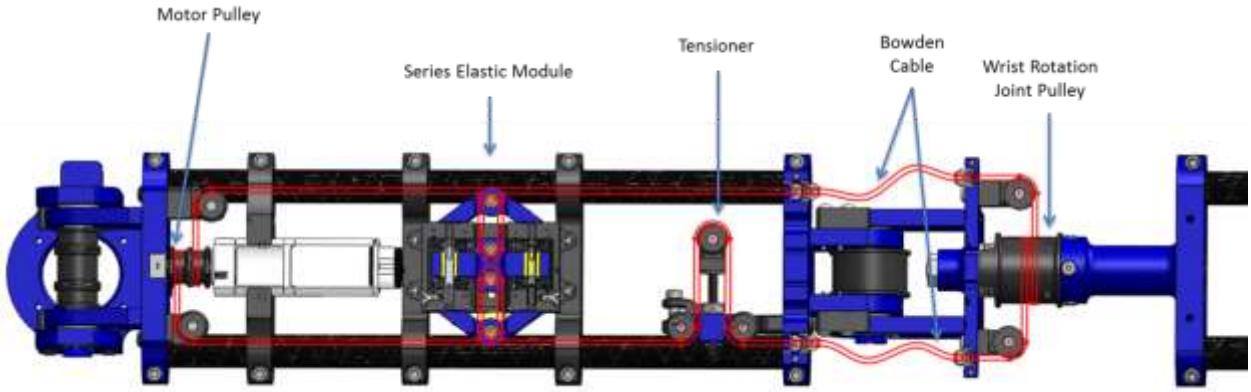

Figure 3-9: Wrist Rotation Cable Routing

Figure 3-9 also shows that the motor for this joint is located in the lower arm and that Bowden cable is used to bridge the gap from the lower arm to the forearm. Both of these decisions were made so that the movement of the wrist rotation joint would be completely separate from the movement of

the preceding two joints. The significance of this decoupling was shown in the inverse kinematics. The shoulder pivot and elbow pivot joints move in the same plane and as such will primarily be moving at the same time. However, the spinning of the wrist rotation joint is completely separate from these two joints. While it is true that the controller will automatically take care of this movement, it was decided that mechanically simplifying the problem was the best solution.

This joint was much simpler to cable compared to the previous two. The tensioner has more travel compared to the shoulder pivot and elbow pivot joints. Therefore nothing special had to be done for cabling aside from terminating the cable on the motor pulley and on the joint. However, if added tension is needed in the future, the Bowden cable can be disconnected to temporarily allow for more slack to be removed.

While it added weight to the lower arm, the motor required to move the wrist rotation joint is much smaller than the other three motors. As such the bonus of not having the wrist rotation joint coupled to the shoulder pivot joint. Furthermore, the effect of the added weight was reduced by locating the motor at the base of the lower arm. Similarly by having the cable pass though Bowden cable instead of wrapping around an idler pulley at the elbow pivot joint results in the wrist rotation joint being completely decoupled from the movement of the elbow joint.

The Bowden cable allows for the decoupling because Bowden cable is able to contain a cable and ensures that the total length of the cable remains the same between the end points while still allowing for 3D motion. The most common application of Bowden cable is on bicycles where the Bowden tubes are used to house the brake and shifter cables. Igus has developed their own version of Bowden cable specifically developed for use with Dyneema and this Bowden cable is being used for the project.

3.2.3 Cable Termination

This project relies upon the use of Dyneema cable. This was chosen based upon the research done in [11] which showed that the Dyneema was cheaper, with a higher yield strength, and a lower coefficient of friction. 1.6 mm diameter cable was used for the arm which has a rated breaking strength of 400 lbs. However, while the low coefficient of friction is beneficial for the idler pulleys, it proved troublesome for cable termination in [11]. Therefore this project focused on finding a reliable method for terminating the Dyneema cable.

Igus developed a successful method for terminating Dyneema using a conical pin which is threaded into the Dyneema. It is then inserted into a plunger, compressing the Dyneema between the two brass pieces. However, the outer piece used by Igus was too large for most of the applications for this arm. Therefore, it was built into the pulley. A 5 degree 1/16" endmill was used to create this hole. Additionally, the wall thickness of the pulley was increased at this location to prevent failure. The Igus cone was then threaded into the Dyneema and sandwiched against the pulley. One of these pulleys is shown in Figure 3-10.

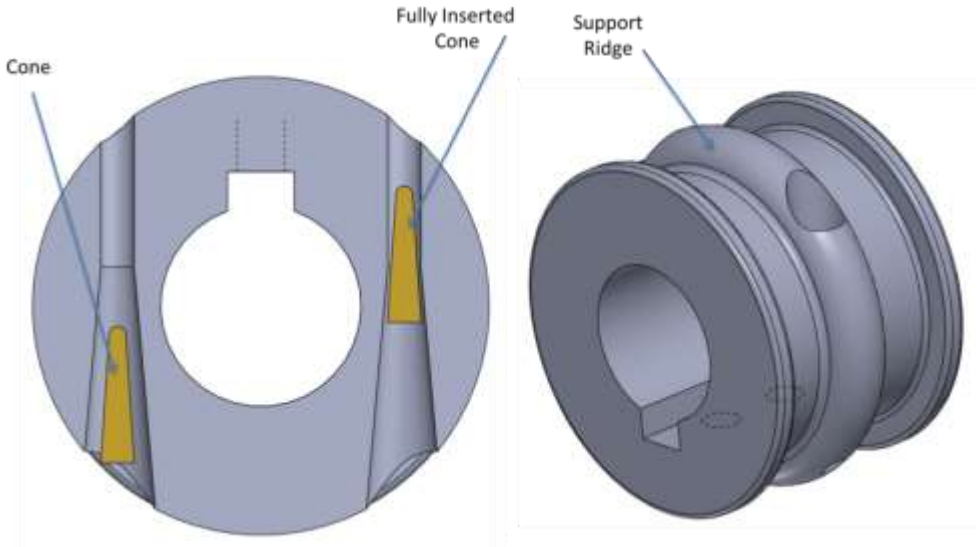

Figure 3-10: Cable Termination

This approach was used on all four of the motor pulleys in addition to the wrist rotation pulley. The complete Igus method was used to terminate the cables in the shoulder rotation, shoulder pivot, and elbow pivot series elastic modules. It was also prototyped and tested on the bipedal walking platform developed in [11]. It was found that this approach, combined with the application of Locktite ensured that the cable would not slip. Since the biped experiences higher forces than those calculated for the arm, it was deemed a valid solution for the arm as well.

3.2.4 Base Design

The base was designed to be as small as possible. It has a diameter of 11 inches and a height of 5.25 inches. The limiting factor for the base was the size of the motors for the shoulder pivot joint and elbow pivot joint and the fact that they must be able to rotate inside the base. The top plate was pocketed to allow for airflow into the base to cool the motors and motor controller. Additionally, provisions were made to allow for tactile sensors to be added to the top plate in the future.

The base plate was designed to be mounted to a table. There is a bolt pattern so that the base can be bolted to a table and there is space for clamps as well. Additionally, the base has been designed to have a removable acrylic plate which the electronics will be mounted to. This was done to allow for easy changes to electrical packaging since a new acrylic plate can be laser cut in minutes from cheap acrylic instead of having to get a new base plate machined. The electrical design and location of components are further discussed in section 3.3.

3.2.5 Tactile Sensor Integration

The primary goal of this project is to investigate the impact of adding tactile sensors to the arm of a robot. However, the focus of this thesis was the development of a compliant platform with consideration for the integration of the tactile sensors. Therefore, only a preliminary shell of tactile

sensors was developed for this project. Additionally, the sensors themselves were not made as part of this thesis while the shell, mold, and rubber exterior were.

3.2.5.1 Tactile Sensor Design

The tactile sensors used for this project are based on those developed on the robots Obrero [9], Go-Bot [8], and Caminante [11]. As explained in Section 1.1.3.2, these tactile sensors provide an inexpensive solution which allows for the detection of both normal and shear forces. The sensors function by having one IR LED and four phototransistors which measure light diffracted off of a semicircular dome. As a force is applied to the dome, it begins to deform. This deformation causes a change in the amount of light measured by each phototransistor. This change in light is then used to determine the magnitude and direction of the force.

3.2.5.2 Shell Design

The shell covers both links of the arm with a decagon 245 mm long, an outer diameter of 100 mm, and a side width of 30.5 mm. To better replicate the human arm, the tactile sensors were made larger than those on the fingers, but still have a resolution higher than the human arm which has a resolution of approximately 40 mm. Each sensor has a diameter of 17 mm spaced 24 mm apart for a total of 10 sensors per side. The shells integrated onto the arm are shown in Figure 3-11. As shown in the figure, the shells provide adequate coverage of the links but the joints are still exposed.

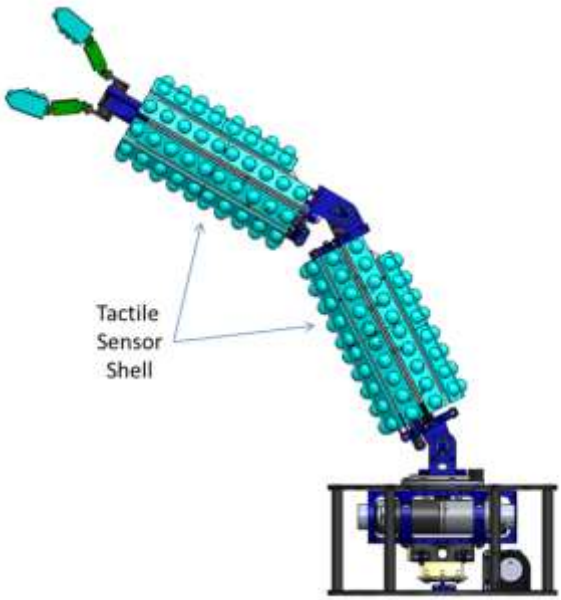

Figure 3-11: Arm with Shell

Focusing on the lower link of the arm, the design of the shell can be analyzed. The shell was designed so that it is the last piece attached to the arm. It was also designed to clamp around the carbon fiber tubes allowing for the most general form of attachment which work for both the lower arm and forearm. An exploded view of the lower arm and the shell is shown in Figure 3-12.

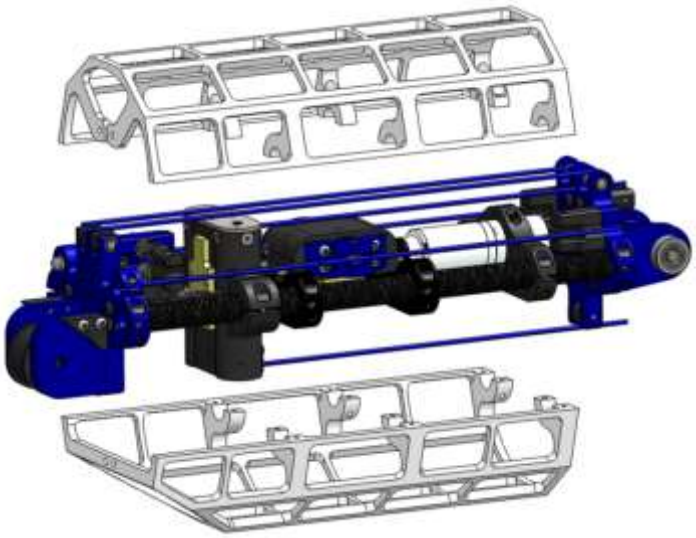

Figure 3-12: Lower Arm Shell

The shell is composed of two halves which primarily clamp to the carbon fiber tubes but are also attached to one of the endplates (left side of the figure). Having a series of rings which all clamp to the tubes was also considered; however, it was found that having two halves instead of several rings allowed for more optimal placement of the tube clamps and greater shell rigidity without an increase in weight. This light weight was made possible by pocketing the shell heavily which also provides ample space to pass the wiring from the tactile sensors to the arm and back to the base and attached computer.

Not only did the shell have to be designed to attach to the arm without interfering with the existing components, but it also could not reduce the range of motion of the arm. Therefore, as shown in Figure 3-11 and Figure 3-12, the shell has notches removed to account for the range of motion of the asymmetrical elbow. The three sections which had to be shortened for these notches have 8 bubbles instead of 10 but the bubbles have the same diameter and spacing.

3.2.5.3 Mold Design

The sensors were purposefully designed to be simple strips so that the tactile shell would be as modular as possible. As a result, the arm is comprised of either 8 dome or 10 dome strips. While the mold for the tactile sensors is rather simple, it is worth mentioning. It is shown in Figure 3-13 and consists of an upper and lower segment.

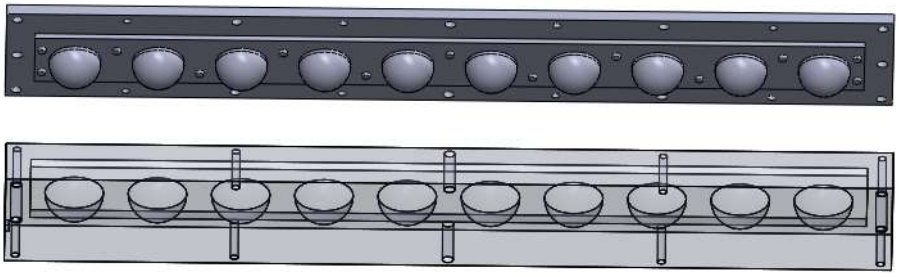

Figure 3-13: Tactile Sensor Mold

The molding process is the same as described in [11], however, research is being performed to reduce light contamination and the escape of the IR light which may be incorporated into these sensors in the near future. In either case, the domes are made from a Freeman V-1062 base and a catalyst.

3.3 Electrical Architecture

The electrical system was designed to best utilize the tactile sensors and series elastic elements. The high level electrical architecture was designed in conjunction with an electrical engineering student who also performed all of the electrical design work. It uses custom motor controllers capable of regulating the position and force for each joint. The processing power is handled outside of the arm on a PC. The mechanical design included two acrylic sheets which electronics could easily be mounted to: one in the base and one on the bottom of the lower arm. A block diagram illustrating the electrical architecture is shown in Figure 3-14.

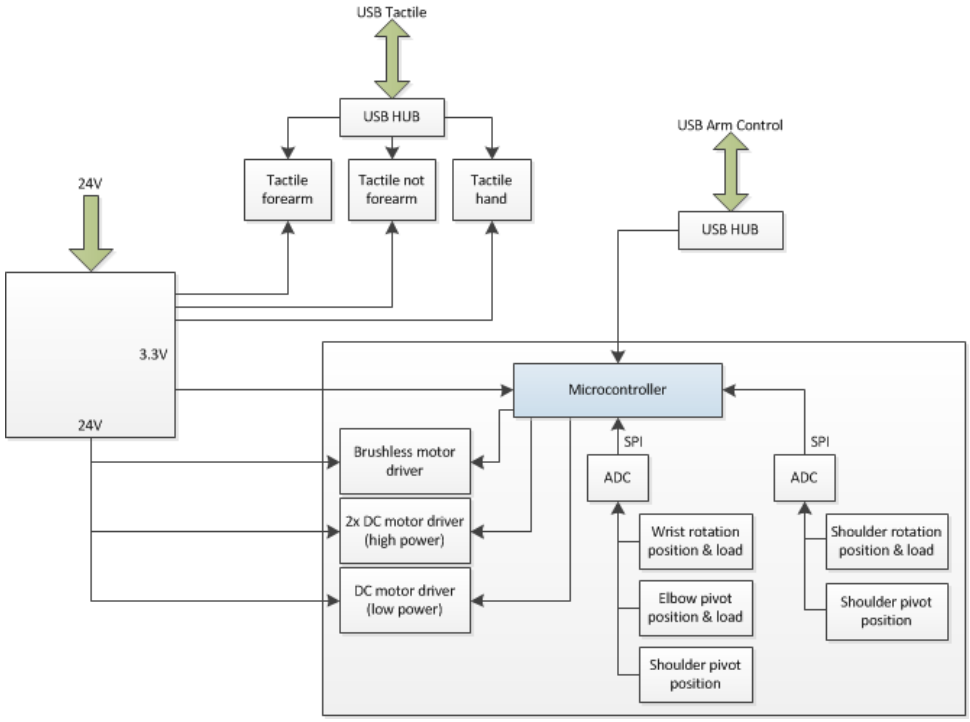

Figure 3-14: Electrical Block Diagram

The PC accumulates data from many different inputs via USB. USB reduces the total number of cables going to the PC and its high transmission rate is needed to respond to the large amount of data coming from the tactile sensors which are each sampled at 100 Hz. The motors are controlled by an LPC2148 microcontroller which reads the linear (for force measurement) and rotary (for position measurement) potentiometers for each joint and runs a PD controller at 1 kHz. One LPC2148 is capable of reading 6 potentiometers and controlling three motors. This controller then outputs the necessary signal to a custom motor driver which provides the necessary current to the motor using a PWM signal. Three of these drivers are for brushed motors while one is for a brushless motor and all of them operate at 24 V. In addition to regulating the voltage to the motors, the drivers also allow for the motors to enter brake mode and hold position.

Since the motors for the two shoulder joints and elbow are located in the base, they share a controller. The potentiometer signals are collected closer to the source, converted to digital signals, and transmitted using SPI to the controller. The controller for the wrist rotation joint is located in the lower arm and also controls the other two wrist joints.

3.4 Manipulation Algorithm

The purpose of this arm is to investigate new methods of manipulation to utilize the increased feedback from tactile sensors located on the arm. One proposed manipulation approach is described in this section. It is important to realize that the approach about to be described only covers the movement of the arm and specifically the joints designed for this thesis. After the process described, a separate process would take place to grab a desired object and manipulate it accordingly. Therefore, this process only covers reaching a goal location and not the handling of an object.

Current manipulation techniques rely upon a pre-existing knowledge of the environment. A trajectory is then developed for the manipulator to follow which ensures that neither the manipulator nor the arm will contact anything in the surroundings. However, in reality, there are some objects which are deformable or easily moved and these aspects cannot be identified via visual sensors. Instead, by allowing the arm to come in contact with its environment, and using the tactile sensors to regulate this interaction, the arm can operate in spaces where a traditional robotic arm would be unable to find a valid path. Additionally, the same algorithm which can be used to regulate the interaction force with stationary objects can also be used to ensure that the robot can safely interact with humans.

The generalized form of the process for navigating the arm is shown in Figure 3-15. The arm tries to keep all interaction forces below a specified acceptable level while still moving towards the goal location. At a lower level, both position and force control are used to regulate motor speeds.

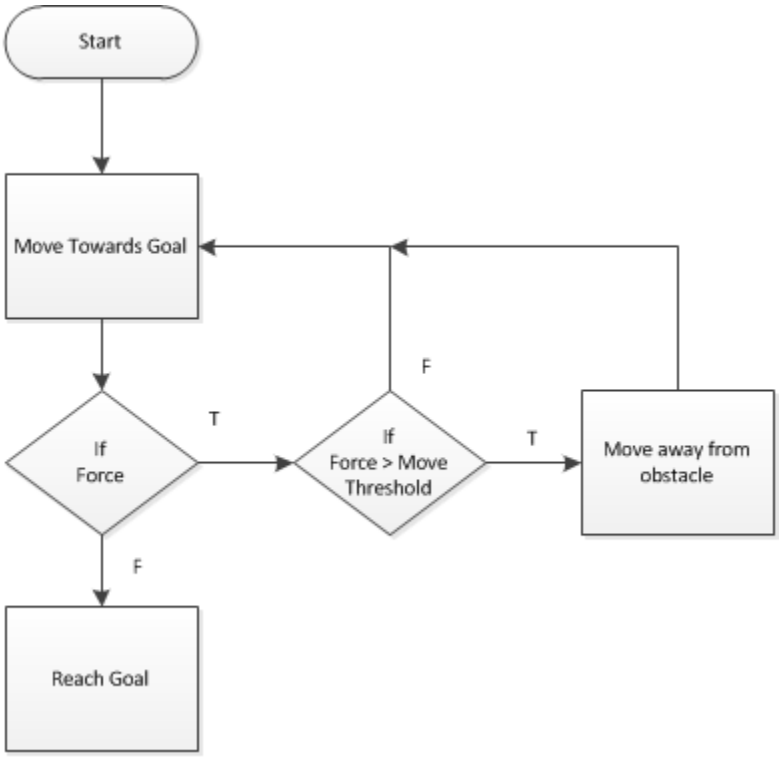

Figure 3-15: Flowchart for Manipulation Decision Process

It would be assumed that the arm has a known goal location and task. For example, the robot may need to take a bag of chips off of a shelf. The location of the chips would be known based upon a vision system. The arm would begin reaching towards the chips, constantly reading the sensor values. It may brush against a box of pasta which does not move. This would register as a low shear force by the sensors. Since the arm is successfully sliding past the box, it would continue. The arm may also push against a bag of popcorn. It would push the popcorn out of the way, registering a normal force, and finally reach the chips. Next, the arm hits the side of the shelf. The force measured by sensors slowly builds. The arm continues moving into the side until the force exceeds a predetermined threshold. At this point the arm begins to move away from the wall to keep the interaction force below the threshold. Finally, the arm is to the point where it can grab the chips. Not part of the algorithm described below but part of the complete task is the fingers then wrap around the chips, gently grabbing the bag by regulating the force measured by the sensors on the fingers. The arm would then retract bringing the chips off of the shelf.

Chapter 4: Evaluation and Analysis

After being fully assembled, the arm and motors were tested. The assembled arm is shown in Figure 4-1. All joints function as intended, however, the shoulder pivot and elbow pivot were found to not generate the expected amounts of torque. The testing procedure consisted of testing the arm with no load, a simulated load, and with a torque wrench instead of motors.

Figure 4-1: Assembled Arm

4.1 Range of Motion

The first step in evaluating the arm was to test all of the joints to ensure they moved as intended. This was done by powering each motor with a controller provided by Maxon. All four of the joints were able to travel over the desired range of motion. However, this did not provide any results beyond a primary system test.

4.2 Simulated Load Testing

In order to determine if the arm could operate as intended, a simulated load had to be applied to account for the lack of the rest of the wrist, the hand, or the payload. It was calculated that attaching a 2.25 kg load to the end of the arm would simulate the missing components and payload. When this payload was added to the arm it was found that the shoulder rotation and wrist rotation joints functioned as expected, however, the shoulder pivot joint could not manipulate the load and the elbow pivot joint required more effort than anticipated.

It was determined that the lever arms such as those shown in Figure 3-5 were not the true lever arms. Instead, it was determined that one of the options depicted in Figure 4-2 was the true lever arm.

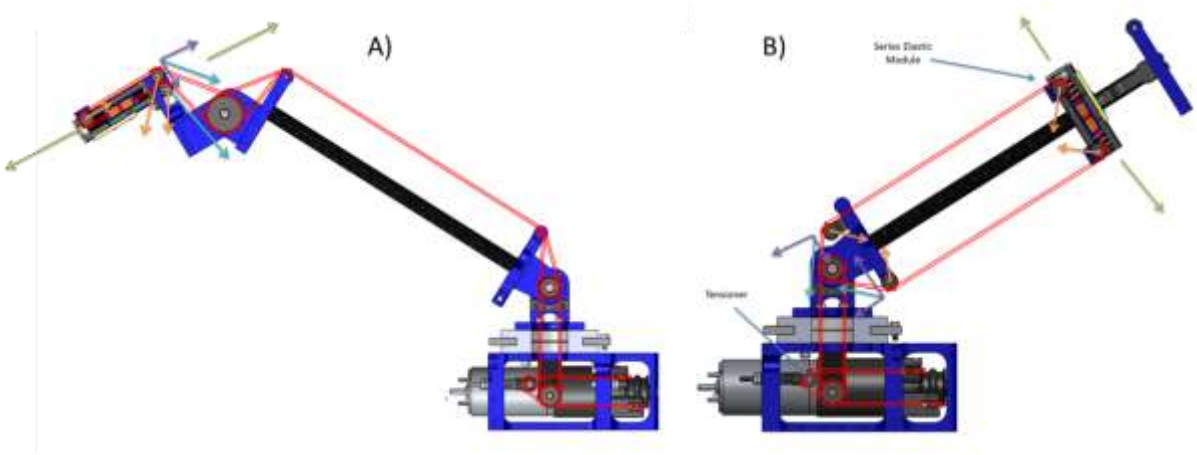

Figure 4-2: Joint Lever Arm Possibilities

The green arrows in Figure 4-2 show where it was thought the tension in the cable was being applied. One option is that this assumption is true; however, the reaction forces on the idler pulleys (shown in orange) were neglected. Specifically, if the cable begins to lose tension, then these reaction forces no longer cancel each other out and must be accounted for. Another option was that the force from the cable is actually being applied at the first idler pulley as shown by the light blue arrow. This force can be broken into its components, shown in purple. Not only does applying the torque at this location greatly reduce the lever arm which the force is applied, but only part of the force generates a torque in the correct direction. Examining the torques generated by these components, it is shown that the components generate torques in opposite directions. Therefore only a fraction of the anticipated torque is being generated. However, additional testing had to be performed in order to determine which of these theories was correct.

4.3 Torque Gauge Testing

In order to accurately determine the torque required to move the arm, the motors and pulleys for the shoulder pivot and elbow pivot joints were replaced by pulleys capable of interfacing with a torque gauge. Additionally, the potentiometers measuring the deflection of the springs for these two joints had their resistances measured using a multimeter. The arm configured to test the shoulder pivot joint is shown in Figure 4-3.

Figure 4-3: Torque Gauge Test

Due to limitations in the torque gauge, the motor rotating in the counterclockwise direction was simulated up to a torque of 6 Nm. Given these limitations, the shoulder pivot and elbow pivot joints were tested and the results shown in Table 4-1 were obtained.

Table 4-1: Torque Gauge Tests

Joint	Configuration	Torque (N*m)	Spring Deflection (mm)
Shoulder Pivot	Elbow in, no load	4.6	0.08
Shoulder Pivot	Elbow out, no wrist rotation spring box	5.7	0.17
Elbow Pivot	No load	0.9	0.03
Elbow Pivot	1.2 kg load	4.6	0.11
Elbow Pivot	1.36 kg load	5.4	0.13

The torque values shown in Table 4-1 were recorded from the torque gauge while the spring deflection was calculated from the readings of the linear potentiometer on each of the joints.

4.4 Determination of Joint Lever Arm

The results from the tests with the torque wrench were compared to the options displayed in Figure 4-2. It was found that the actual lever arms for these two joints occur at the first pulley the cable comes in contact with (the light blue and purple arrows shown in Figure 4-2). The calculations and additional figures required to come to this conclusion is shown in Appendix E. The calculations in Appendix E show that, after accounting for the efficiency of the cable and inaccuracies in the torque gauge, the lever arm transferring the motor torque to the arm is less than anticipated for the shoulder pivot and elbow pivot joints. The accurate lever arms are shown with the light blue arrows in Figure 4-2.

4.5 Joint Torque Solutions

Given that the arm cannot generate enough torque in its current configuration, there are several options for the future development of the arm. The easiest solution would be to simply reduce the payload the arm operates. However, the arm can be easily modified to maintain full functionality. The most likely alternative is to replace the motor and gearbox with a combination of developing more torque and replacing the springs with stiffer alternatives. The exact same motor and a gearbox with the same efficiency and dimensions can be obtained with a gear ratio of 156:1 instead of 43:1. Therefore, without requiring any modification the torque generated for both of these joints can be tripled. Additionally, due to the modular nature of the series elastic elements, there are many different stiffer springs which can be integrated into the modules with little to no alteration.

A final possibility is to redesign both of the joints so that the cable only travels in 90 degree increments thereby eliminating the cable force generating conflicting torques. Furthermore, a larger

pulley could be incorporated into the shoulder pivot joint to help reduce the spring rate required. This solution would need to be implemented in conjunction with an increase in motor torque and spring stiffness.

Chapter 5: System Validation

To evaluate the soundness and success of the designed arm, shown in Figure 5-1, it was thoroughly tested. These tests were constructed so that the results correlated with the design requirements specified in Section 3.1. The general process for these experiments was to operate the arm with a payload and compare the joint deflection to those expected in the dynamic simulation. The results of this system validation are shown in the subsequent sections.

Figure 5-1: Complete First Four DOF of Robotic Arm

5.1 Manipulate 1 kg Payload

One of the requirements for this system was to make it capable of handling a one kilogram payload. However, this could not be directly tested since the rest of the arm had not been constructed at the time of testing. Therefore, a mock payload of five pounds was added to the arm. The location and weight of this payload were selected to have the same effect as the 1 kg payload as well as the missing weight of the forearm, wrist, and hand.

Three of the four joints were successfully able to manipulate this payload. The fourth joint, the shoulder pivot joint, was unable to manipulate the 2.25 kg payload but was able to manipulate a 1.2 kg payload representing the mass of the arm and hand in all but the most extreme cases. Therefore, the arm is acceptably functional but cannot manipulate the required 1 kg payload. Without having to perform any modification to the arm, the motor and gearbox can be replaced allowing the arm to manipulate the arm as intended and with minimal joint modifications will be able to manipulate the arm and 1 kg payload.

5.2 Size of Small Human Arm

The arm was designed to approximately replicate the size of a small human arm. This was achieved by having two links each 0.3 m in length. Additionally, in its current configuration, the arm and base have a combined mass of 9 kg and the arm on its own has as mass of 2.25 kg. This light weight of the arm can be attributed to the design decision to place the motors for the shoulder and elbow in the stationary base. Addition of the wrist and hand is estimated to add an additional 2 kg for an arm mass of 4.25 kg and a total mass of 11 kg. Therefore, the size and weight of the arm excluding the base approximate that of a small human arm.

5.3 Tactile Sensor Coverage

The ultimate purpose of this arm is to perform manipulation tasks with an arm covered in tactile sensors. Therefore, the requirement to adequately cover the tactile sensors was an important consideration. The arm was designed to provide mounting points for a shell of tactile sensors. A prototype shell was also developed for the lower arm and contained 100 tactile sensors spread across ten sides of a decagon. Additionally, one of these strips of tactile sensors was molded to demonstrate

this coverage. The density of tactile sensors proves to be much more than that of a human arm (40 mm per sensor) and therefore is satisfactory.

5.4 Degrees of Freedom

The arm was designed to replicate a human arm in terms of the degrees of freedom. Therefore, it has a two degree of freedom shoulder, one degree of freedom elbow, and three degree of freedom wrist. However, unlike a human arm, the rotation of the wrist occurs near the elbow instead of near the wrist itself. The shoulder, elbow, and rotation element of the wrist were all successfully implemented for this project while the other two degrees of freedom and a hand are a separate project.

5.5 Easily Assembled SEA Modules

A heavy emphasis was placed upon the design of the series elastic actuators. They had to be easily assembled and, preferably, comprised of separate modules which are assembled and integrated into the arm. This was accomplished in the shoulder pivot, elbow pivot, and wrist rotation joints. The shoulder rotation joint was also easily assembled but could not be assembled separately from the arm.

All four joints are capable of being safely assembled by a single person. The shoulder pivot, elbow pivot, and wrist rotation joints are self-contained which has the benefit of modularity. The shoulder rotation joint is not modular but temporarily utilizes bolts to easily compress the spring. While not as well packaged, the shoulder rotation joint was the easiest joint to tension since the springs ensure tension in the entire joint. Additionally, the wrist rotation joint is unique because it can be incorporated anywhere in the cable system as opposed to other SEAs which must be implemented at either the motor or the joint. The design for the wrist rotation joint therefore helps reduce the size of the system by allowing the SEA to be placed in the most convenient or compact location.

5.6 Joint Deflection

The joint deflection was designed to replicate that of a human. Therefore the range of motion had to meet or exceed that of a human and more noticeably, the elbow had to be asymmetrical. As shown in Table 5-1, each joint successfully replicates its human counterpart.

Table 5-1: Joint Range of Motion

Joint	Robotic Arm (deg)	Human Arm (deg)
Shoulder Rotation	140 to -140	0 to 270
Shoulder Pivot	75 to -75	0 to 100
Elbow Pivot	140 to -40	0 to 140
Wrist Rotation	105 to -105	0 to 180

Table 5-1 shows that the shoulder rotation and shoulder pivot joints exceeds the motion of a human. Additionally, the elbow is asymmetrical while still having a larger range of motion in one directions compared to a human. Lastly, the wrist rotation joint allows for the wrist to rotate slightly more than 180 degrees beating a human wrist.

5.7 Hand Integration

This thesis was only one part of the design of a complete arm and hand system which integrated tactile sensors. Therefore, the first four joints of the arm developed for this thesis had to successfully integrate with the components needed for the additional degrees of freedom in the wrist as well as the hand and fingers. To accomplish this, the wrist rotation joint was incorporated into the elbow. Carbon fiber tubes, such as those used in the lower arm, then protruded from this joint providing a simple mounting surface for all additional hardware. The electrical architecture was also designed so that minimal wiring had to be passed to the forearm while still allowing for full functionality of the wrist and hand.

5.8 Overall System Performance

Each component of the system has been thoroughly tested. Every joint has been moved across its full range of motion and carrying a payload simulating extreme operating conditions under its own power. The robustness of the joints has also been tested with the same payload to ensure that collisions do not harm the robot. The arm has found to successfully meet almost all of the design criteria. The one exception is the ability to manipulate a 1 kg payload in all possible configurations. Three out of the four joints are able to fulfill this goal and an easy solution has been proposed to allow the fourth joint to achieve this goal as well.

Chapter 6: Conclusion and Future Work

Finally, the contributions of this thesis are presented along with a plan for future progress. The contributions show that the goals of the project were met in the development of a platform to further mature the concept of sensitive manipulation through the inclusion of tactile sensors on a compliant arm. The future work describes the short term and long term tasks required for the project.

6.1 Conclusion

This thesis presented the design of a robotic arm utilizing series elastic actuators in every joint and which incorporated a shell of tactile sensors to perform sensitive manipulation. The SEAs added compliance to the arm to aid in this contact based approach to manipulation and were designed to be modular and easily assembled. The tactile sensors are capable of detecting normal and shear forces and therefore can be used to identify and regulate both pushing and sliding interaction forces.

In the process of this design, kinematic and dynamic models of the arm were developed. The forward and inverse kinematics were used for the dynamic model but can also be utilized in the implementation of control algorithms. The dynamic model was used to determine joint torques which allowed for the selection of motors and springs. The electrical architecture needed to power the motors and read the sensors for the SEAs and tactile system was also discussed. Finally, the high level procedure for utilizing the tactile sensors in a manipulation task was covered along with an example.

6.2 Future Work

Despite careful attention to detail in the design process, the evaluation uncovered a flaw with design which limited the capabilities of the shoulder pivot and elbow pivot joints. Additional analysis

was performed using a torque gauge to determine the true functionality of these joints and a simple repair was proposed which can restore complete functionality.

In addition to the work already done, there is still much more to be done on this arm. The other degrees of freedom of the wrist and the entire hand and fingers have yet to be manufactured but are in the late design stages. Additional work must also be performed on the electronics of the system. Furthermore, only a preliminary shell for the tactile sensors has been developed for the lower arm. A shell for the forearm must still be created and both shells can be made to provide better coverage of the arm. Mounting locations were also provided for tactile sensors to be attached to the top of the base but these have not yet been designed. After these hardware tasks are complete, manipulation algorithms can be tested using the arm to demonstrate the added benefit of tactile sensors incorporated into the arm of a robot. The tasks needed to reach this point are:

- Replace motor and gearbox for shoulder pivot and elbow pivot joints
- Construct wrist and hand
- Complete design and assembly of electrical components
- Design tactile shell with greater coverage of arm
- Design tactile sensors for top of base
- Implement and evaluate manipulation algorithms
- Redesign shoulder pivot joint for increased payload

This thesis resulted in a platform to further develop sensitive manipulation. Much hard work is needed to transform this platform into solid results, demonstrating the potential impact greater sensor integration poses for robotic systems. It is not a coincidence that sensitive manipulation attempts to more closely replicate the sensors present in nature and one day robots will meet and exceed the abilities of their natural counterparts.

References

[1] "World Robotics- Industrial Robots 2012," 2012.

[2] I. Karabegovic, E. Karabegovic, and E. Husak, "Trend of Industrial Robot Share in Different Branches of Industry in America," *IJERA*, vol. 2, no. 2, pp. 479–485, 2012.

[3] J. Pratt, B. Krupp, and C. Morse, "Series elastic actuators for high fidelity force control," *Industrial Robot: An International Journal*, vol. 29, no. 3, pp. 234–241, 2002.

[4] E. Kemp, CC, Edsinger, A, Torres-Jara, "Challenges for robot manipulation in human environments," *Robotics & Automation Magazine*, pp. 20–29, 2007.

[5] A. M. Dollar, L. P. Jentoft, J. H. Gao, and R. D. Howe, "Contact sensing and grasping performance of compliant hands," *Autonomous Robots*, vol. 28, no. 1, pp. 65–75, Aug. 2009.

[6] "RoboSKIN Project." [Online]. Available: http://www.roboskin.eu/index.php.

[7] J. M. Romano, K. Hisiao, G. Niemeyer, S. Chitta, and K. J. Kuchenbecker, "Human-inspired robotic grasp control with tactile sensing," *IEEE Transactions on Robotics*, vol. 27, no. 6, pp. 1067–1079.

[8] E. Torres-Jara and G. Gomez, "Fine sensitive manipulation," *Australasian Conference on Robotics and Automation*, 2008.

[9] E. Torres-Jara, "Sensitive manipulation," 2007.

[10] L. Natale and E. Torres-Jara, "A sensitive approach to grasping," *Proceedings of the sixth international workshop on epigenetic robotics*, pp. 87–94, 2006.

[11] V. Chernyak, "The Design and Realization of a Sensitive Walking Platform," 2012.

[12] "History of Industrial Robots," 2012.

[13] C. Ott, O. Eiberger, W. Friedl, U. Hillenbrand, C. Borst, S. Kielh, R. Konietschke, F. Zacharias, and G. Hirzinger, "A humanoid two-arm system for dexterous manipulation," *Humanoid Robots, 2006 6th IEEE-RAS International Conference on*, pp. 276–283, 2006.

[14] A. Edsinger, "Robot Manipulation in Human Environments," 2007.

[15] E. Guizzo and E. Ackerman, "The Rise of the Robot Worker," *Spectrum, IEE*, vol. 49, no. 10, pp. 34–41, 2012.

[16] M. Williamson, "Series elastic actuators," 1995.

[17] G. Pratt, M. Williamson, P. Dillworth, J. Pratt, and A. Wright, “Stiffness isn’t everything,” *Experimental Robotics*, 1997.

[18] S. Haddadin and F. Huber, “Intrinsically elastic robots: The key to human like performance,” *Intelligent Robots …*, pp. 4270–4271, 2012.

[19] E. Torres-Jara and J. Banks, “A simple and scalable force actuator,” 2005.

[20] R. S. Johansson and R. H. LaMotte, “Tactile detection thresholds for a single asperity on an otherwise smooth surface.,” *Somatosensory research*, vol. 1, no. 1, pp. 21–31, Jan. 1983.

[21] A. Jain, M. Killpack, A. Edsinger, and C. Kemp, “Manipulation in Clutter with Whole-Arm Tactile Sensing,” *Under Review*, pp. 1–20, 2011.

[22] P. Haggard, M. Taylor-Clarke, and S. Kennett, “Tactile perception, cortical representation and the bodily self,” *Current Biology*, pp. 170–173, 2003.

[23] B. D. Argall and A. G. Billard, “A survey of Tactile Human–Robot Interactions,” *Robotics and Autonomous Systems*, vol. 58, no. 10, pp. 1159–1176, Oct. 2010.

[24] B. Sicilano and O. Khatib, “Force and Tactile Sesors,” *Spring Handbook of Robotics*.

[25] J. Jockusch, J. Walter, and H. Ritter, “A tactile sensor system for a three-fingered robot manipulator,” *Robotics and Automation*, 1997.

[26] E. Torres-Jara, I. Vasilescu, and R. Coral, “A soft touch: Compliant tactile sensors for sensitive manipulation,” 2006.

[27] M. Fumagalli, S. Ivaldi, and M. Randazzo, “Force feedback exploiting tactile and proximal force/torque sensing,” *Autonomous Robots*, vol. 33, no. 4, pp. 381–398, Apr. 2012.

[28] A. Edsinger-Gonzales and J. Weber, “Domo: a force sensing humanoid robot for manipulation research,” *4th IEEE/RAS International Conference on Humanoid Robots, 2004.*, vol. 1, pp. 273–291, 2004.

[29] T. Kuiken, “A prosthetic arm that ‘feels’,” *TED Global Confrence*, 2011.

[30] M. K. O’Malley and R. O. Ambrose, “Haptic feedback applications for Robonaut,” *Industrial Robot: An International Journal*, vol. 30, no. 6, pp. 531–542, 2003.

[31] M. Diftler and J. Mehling, “Robonaut 2-the first humanoid robot in space,” *Robotics and Automation (ICRA), 2011 IEEE International Conference on.*, vol. 1, pp. 2178–2183, 2011.

[32] “DLR Institute of Robotics and Mechatronics - Justin.” [Online]. Available: http://www.dlr.de/rm/en/desktopdefault.aspx/tabid-5471/8991_read-16694/.

[33] M. Grebenstein, A. Albu-sch, T. Bahls, M. Chalon, O. Eiberger, W. Friedl, R. Gruber, S. Haddadin, U. Hagn, R. Haslinger, H. Hannes, J. Stefan, M. Nickl, A. Nothhelfer, F. Petit, J. Reill, N. Seitz, T. Wimb, S. Wolf, and W. Tilo, “The DLR Hand Arm System,” pp. 3175–3182, 2011.

[34] W. Friedl, H. Hppner, F. Petit, and G. Hirzinger, “Mechanical Design , Shape Analysis and Experimental Validation Wrist and Forearm Rotation of the DLR Hand Arm System :,” pp. 1836–1842, 2011.

[35] R. Brooks and C. Breazeal, “The Cog project: Building a humanoid robot,” *Computation for metaphors, analogy, and agents*, pp. 52–87, 1999.

[36] C. Breazeal, “Robot in society: friend or appliance,” *Proceedings of the 1999 Autonomous Agents Workshop on Emotion-Based Agent Architectures*, 1999.

[37] “Edsinger Domo.” [Online]. Available: http://people.csail.mit.edu/edsinger/domo.htm.

[38] “Obrero.” [Online]. Available: http://people.csail.mit.edu/etorresj/robot-obrero/.

[39] E. Torres-Jara, “Obrero: a platform for sensitive manipulation,” *5th IEEE-RAS International Conference on Humanoid Robots, 2005.*, pp. 327–332, 2005.

[40] “KUKA Industrial Robots - Arm Tutorial 2.” [Online]. Available: http://www.kuka-robotics.com/usa/en/products/software/educational_framework/arm_tutorials/PS_Content_Arm2.htm.

[41] M. Spong, S. Hutchinson, and M. Vidyasagar, *Robot Modeling and Control*. New York: Wiley, 2006.

[42] H. Høifødt, “Dynamic Modeling and Simulation of Robot Manipulators,” 2011.

[43] P. I. Corke, *Robotics, Vision & Control*. Springer, 2011.

Appendix A: Forward Kinematics

```
function [T A T03 T36 Arm] = forwardKinematics(j1, j2, j3, j4, j5, j6, Arm)
%% convert to radians
j1 = j1*pi/180;
j2 = j2*pi/180;
j3 = j3*pi/180;
j4 = j4*pi/180;
j5 = j5*pi/180;
j6 = j6*pi/180;

j = [j1 j2 j3 j4 j5 j6]';
%% Setting up Matrices
%declare link lengths
%note reference frame of the robot is at first joint

%add an offset to raise the origin above 0,0,0
Offset = [0 0 -.152];

%get DH parameters from the arm
dh = Arm{1};

dh(:,4) = dh(:,4) + j;

%% Create Matricies
forloop = size(dh);
A =cell(1,forloop(1));
%Create array of transformation matricies
%|ai | alphai | di | thetai |
for i = 1: forloop(1);
A{i} = [cos(dh(i,4)) -sin(dh(i,4))*cos(dh(i,2)) sin(dh(i,4))*sin(dh(i,2))
dh(i,1)*cos(dh(i,4));...
    sin(dh(i,4)) cos(dh(i,4))*cos(dh(i,2)) -cos(dh(i,4))*sin(dh(i,2))
dh(i,1)*sin(dh(i,4));...
    0 sin(dh(i,2)) cos(dh(i,2)) dh(i,3);...
    0 0 0 1];
end
%% Multiply matricies together
T = A{1};
for i=2:forloop(1)
    T = T*A{i};
end
%% Duplicate Array
B =cell(1,forloop(1));
for i = 1: forloop(1)
    B{i} = A{i};
end
ROT = cell(1, 6);
ROT = {A{1} A{2} A{3} A{4} A{5} A{6}};
Arm{4} = ROT;
T03 = A{1}*A{2}*A{3};%*A{4};
T36 = A{4}*A{5}*A{6};
A{2} = A{1}*A{2};
```

```
A{3} = A{2}*A{3};
A{4} = A{3}*A{4};
A{5} = A{4}*A{5};
A{6} = A{5}*A{6};
Arm{5} = A;
%% generate figure
%check if J1 is symbolic, should replace with more concrete symbolic plot
%protection
s = size(symvar(j1));
if s(1) == 0
xLine = [Offset(1) 0 A{1}(1,4) A{2}(1,4) A{3}(1,4) A{4}(1,4) A{5}(1,4)
A{6}(1,4)];
yLine = [Offset(2) 0 A{1}(2,4) A{2}(2,4) A{3}(2,4) A{4}(2,4) A{5}(2,4)
A{6}(2,4)];
zLine = [Offset(3) 0 A{1}(3,4) A{2}(3,4) A{3}(3,4) A{4}(3,4) A{5}(3,4)
A{6}(3,4)];

xJoint = [0 A{1}(1,4) A{2}(1,4) A{3}(1,4) A{4}(1,4) A{5}(1,4) A{6}(1,4)];
yJoint = [0 A{1}(2,4) A{2}(2,4) A{3}(2,4) A{4}(2,4) A{5}(2,4) A{6}(2,4)];
zJoint = [0 A{1}(3,4) A{2}(3,4) A{3}(3,4) A{4}(3,4) A{5}(3,4) A{6}(3,4)];

%% Generate coord Frames

XCoord = [Offset(1) 0 A{1}(1,4) A{2}(1,4) A{3}(1,4) A{4}(1,4) A{5}(1,4)
A{6}(1,4)];

figure1 = figure;
PlotLine = plot3(xLine,yLine,zLine);
hold on
for i = 1:forloop(1)
    scale = .07;
    X = A{i}*[scale;0;0;1];
    Y = A{i}*[0;scale;0;1];
    Z = A{i}*[0;0;scale;1];
    Frame1X = [A{i}(1,4) X(1,1)];
    Frame1Y = [A{i}(2,4) X(2,1)];
    Frame1Z = [A{i}(3,4) X(3,1)];
    plotCoords = plot3(Frame1X,Frame1Y,Frame1Z);

    set(plotCoords,'LineWidth',2,'Color',[0 1 0]);
    Frame1X = [A{i}(1,4) Y(1,1)];
    Frame1Y = [A{i}(2,4) Y(2,1)];
    Frame1Z = [A{i}(3,4) Y(3,1)];
    plotCoords = plot3(Frame1X,Frame1Y,Frame1Z);

    set(plotCoords,'LineWidth',2,'Color',[1 0 0]);
    Frame1X = [A{i}(1,4) Z(1,1)];
    Frame1Y = [A{i}(2,4) Z(2,1)];
    Frame1Z = [A{i}(3,4) Z(3,1)];
    plotCoords = plot3(Frame1X,Frame1Y,Frame1Z);
    set(plotCoords,'LineWidth',2,'Color',[.5 0 .5]);
end

PlotPoints = plot3(xJoint,yJoint,zJoint);
set(PlotPoints,'MarkerFaceColor',[1 0 0],'MarkerEdgeColor',[0 0 0],...
```

```
    'Marker','o',...
    'LineWidth',2,...
    'LineStyle','none',...
    'Color',[1 0 0]);
set(PlotLine,'LineWidth',4,'Color',[0 0 1]);
axis([-.4 .4 -.4 .4 -.4 .4]);
%axes('x','y','z');
xlabel('x (m)');
ylabel('y (m)');
zlabel('z (m)');
% Create title
title('Robot Arm Kinematics');
end
end
```

Appendix B: Inverse Kinematics

```
%% Inverse Kinematics
% Takes an x, y, and z coordinates
% Takes pos matrix
% Returns joint angle vector (JA) in degrees
function JA = inverseKinematics(Pos, Arm)
%declare link lengths
%note reference frame of the robot is at first joint
%  a2 = 0.304;
% a3 = 0.021;
% d4 = 0.3137;
l1 = 0.021;
l2 = 0.3137;
x = Pos(1,4);
y = Pos(2,4);
z = Pos(3,4);
a2 = Arm{1}(2,1);
a3prime = sqrt(l1^2+l2^2);
%a3prime = Arm{1}(3,1);

T03 = Arm{5}{3};

%% Find theta 1
JA = zeros(1,6);
JA(1) = atan2(y,x);
%% Find Theta 3
D = (x^2+y^2+z^2-a3prime^2-a2^2)/(2*a3prime*a2);
theta3Pos = atan2(D,sqrt(1-D^2));
theta3Neg = atan2(D,-sqrt(1-D^2));
% Choose whether elbow up or elbow down
if theta3Neg > theta3Pos
    theta3prime = theta3Pos;
else
    theta3prime = theta3Neg;
end
% JA(3) = atan2(d4,a3)-theta3prime;
JA(3) = pi/2-theta3prime;
%% Find Theta 2
%d = atan2(a2+d4*cos(JA(3)),d4*sin(JA(3)));
d = atan2(a2+a3prime*cos(JA(3)),a3prime*sin(JA(3)));
JA(2) = -atan2(sqrt(x^2+y^2),z) + d;
%JA(2) = atan2(z,x) - d;
%% Delete last column and bottom row of Pos
Pos(:,4) = [];
Pos(4,:) = [];
T03(:,4) = [];
T03(4,:) = [];
%% Multiply Pos by the transpose of the Arm
Pos = T03.'*Pos;
X = Pos(1,3)^2;
Y = Pos(2,3)^2;
Z = Pos(3,3)^2;
%% Find Theta 4
```

```
JA(4) = atan2(Pos(2,2),Pos(1,2));
%% Find Theta 5
JA(5) = atan2(sqrt(1-Pos(3,2)^2),Pos(3,2));
%% Find Theta 6
JA(6) = pi + atan2(Pos(3,3),Pos(3,1));
%% Convert to degrees
JA=JA.*180/pi;
end
```

Appendix C: Dynamics

```
% Takes a trajectory and an Arm configuration and returns the torques
function [t Arm] = dynamics(Q, Arm)
%% initial values
%position, velocity, acceleration
q = Q(1,:);
qd = Q(2,:);
qdd = Q(3,:);

joints = size(q,2); % number of joints
n = joints;

z0 = [0 0 1]';% z vector
x0 = [1 0 0]';% x vector
g0 = [0 0 10]';%gravity
f0 = [0 0 0]'; %external tip force
t0 = [0 0 0]';%external tip torque
a = [0 0 0]';%angular acceleration
w = [0 0 0]';%angular velocity

ae = g0;

Fm = cell(1,joints);%intermediate step
Nm = cell(1,joints);%intermediate step

t = zeros(1,joints); %joint torque

%% r vector
%each row is a separate joint
%get the link lengths from the d-h parameters
link = Arm{1}(:,1);
%location of center of mass

%ri,ci center of mass from tip
rci = Arm{2};

%ri-1,i base to tip
%sz = size(rci,2);
ri1_i = cell(1,joints);
ri1_ci = cell(1,joints);
for i = 1: joints
    ri1_i{i} = x0*link(i);
    ri1_ci{i} = ri1_i{i} + rci{i};
end

%% next section
%mass
m = Arm{6};

%intertia
I = Arm{3};
```

```
%% forward kinematics to update rotation matrices
    [T Arm] = forwardKinematics(q, Arm);
    %rotation from i-1 to i
    R = Arm{4};

    %rotation from 0 to i
    R0 = Arm{5};

    %make into rotation matrices instead of transformation
    for i = 1 : (size(R,2))
        R{i}(:,4) = [];
        R{i}(4,:) = [];
        R0{i}(:,4) = [];
        R0{i}(4,:) = [];
    end
%% forward recursion
        %forward
        for i = 1:n
            %initialize variables all seem fine
           bt = ri1_i{i};
           cm = rci{i};
           Rm = R{i};
           Rt = Rm';

           %evaluate
           a = Rt * (a + z0 * qdd(i) + cross(w, z0*qd(i)));
           w = Rt * (w + z0*qd(i));

           ae = Rt*ae + cross(a, bt) + cross(w, cross(w, bt));
           ac = ae + cross(a, cm) + cross(w, cross(w, cm));
           F = m{i} * ac;%intermediate step so store less variables
           N = I{i} * a + cross(w, I{i} * w);%intermediate step so store less
variables
           Fm{i} = F;%intermediate step so store less variables
           Nm{i} = N; %intermediate step so store less variables
        end

%% backward recursion
        %backward
        f = f0; % include external force
        T = t0; %external torque

        for i = n:-1:1
            %account for first step
            if i == n
                Rm = eye(3,3);
            else
                Rm = R{i+1};
            end

            %initialize variables
           bt = ri1_i{i};
           cm = rci{i};
           Rt = Rm';
```

```
            %execute

            T = Rm * (T + cross(Rt * bt, f)) + cross(bt + cm, Fm{i}) + Nm{i};%
torque vector
            f = Rm*f + Fm{i};%force vector

            Rm = R{i};
            t(i) = T'*( Rm' * z0);%joint torque


        end
end
```

Appendix D: Spring and Motor Selection

Wrist Rotate

$T_{total} := 0.78N \cdot m$ — calculated from dynamic model

$\omega_a := \pi \frac{rad}{s} = 30 \cdot rpm$

Spring

$r := \frac{.625}{2} in = 0.313 \cdot in$ — EFFECTIVE radius of the springs (the lever arm of the spring for torque)

$cir := 2\frac{1}{2} in \cdot \pi = 3.142 \cdot in$ — circumfrence of the pulley (fraction is the radius of the idler pulley about the point of rotation)

$deflection := 5deg$ — the desired deflection at the maximum dynamic load

$travel := cir \cdot \frac{deflection}{360deg} = 0.044 \cdot in$ — the distance the spring should deflect at the max dynamic load

$F_{full} := \frac{T_{total}}{r} = 22.091 \cdot lbf \quad F_{full} = 98.268 \cdot N$ — the spring force required to counteract the maximum dynamic load

$k := \frac{F_{full}}{2 \cdot travel} = 253.15 \cdot \frac{lbf}{in}$ — the spring constant required to satisfy the desired force at the desired deflection (the 1/2 is because of having the two springs at half compression)

$k_{parallel} := \frac{k}{2} = 126.575 \cdot \frac{lbf}{in}$ — the required spring force if using two springs in parallel

$def_{max} := 15deg$ — the desired joint deflection when the spring bottoms out

$travel_{max} := cir \cdot \frac{def_{max}}{360deg} = 0.131 \cdot in$ — this is the maximum movement of the spring in one direction based on the maximum desired deflection above)

$f_{max} := travel_{max} \cdot k = 33.137 \cdot lbf$ — the maximum force generated when the spring is fully compressed

$travel_{full} := travel_{max} \cdot 2 = 0.262 \cdot in$ — this is the total amount of deflection the spring must be capable of because it must move in two directions

Motor

Desired Specs:

$T_{total} = 0.78 \cdot N \cdot m$

$S_1 := \omega_a = 30 \cdot rpm$

Pulley Gear Ratio

$pulley := \frac{r \cdot 2}{.5in} = 1.25$

$T_{pulley} := \frac{T_{total}}{pulley} = 0.624 \cdot N \cdot m$ $\qquad T_{safe} := T_{pulley} \cdot 1.75 = 1.092 \cdot N \cdot m$

$S_{pulley} := S_1 \cdot pulley = 37.5 \cdot rpm$

Gearbox:

$ratio := 231 \qquad efficiency := .65$

$T_{motor} := \frac{\frac{T_{safe}}{ratio}}{efficiency} = 7.273 \cdot 10^{-3} \cdot N \cdot m$

$S_{motor} := S_{pulley} \cdot \frac{ratio}{efficiency} = 13326.923 \cdot rpm$

Given the above specs, chose motor with:

$Motor_T := 15.1 \cdot 10^{-3} N \cdot m \quad Motor_S := 12400 rpm$

$T_{motor} := Motor_T \cdot ratio \cdot efficiency = 2.267 \cdot N \cdot m$

$T_{motor} - T_{safe} = 1.175 \cdot N \cdot m$

$S_{motor} := \frac{Motor_S}{ratio} \cdot efficiency = 34.892 \cdot rpm$

$S_{motor} - S_{pulley} = -2.608 \cdot rpm$

$T_{motor} > T_{safe} = 1$

$S_{motor} > S_{pulley} = 0$

Elbow

$T_{total} := 11.7N \cdot m \qquad \omega_a = 30 \cdot rpm$

Spring

$r := 1.94in = 0.049\,m$

$cir := 2 \cdot \frac{1.125}{2} in \cdot \pi = 3.534 \cdot in$

$deflection := 5deg$

$travel := cir \cdot \frac{deflection}{360deg} = 0.049 \cdot in$

$F_{full} := \frac{T_{total}}{r} = 53.378 \cdot lbf \qquad F_{full} = 237.438 \cdot N$

$k := \frac{F_{full}}{2 \cdot travel} = 543.706 \cdot \frac{lbf}{in}$

$\frac{k}{2} = 271.853 \cdot \frac{lbf}{in}$

$def_{max} := 15deg$

$travel_{max} := cir \cdot \frac{def_{max}}{360deg} = 0.147 \cdot in$

$f_{max} := travel_{max} \cdot k = 80.067 \cdot lbf$

$travel_{full} := travel_{max} \cdot 2 = 0.295 \cdot in$

Motor

Desired Specs:

$T_{total} = 11.7 \cdot N \cdot m$

$S_1 := \omega_a = 30 \cdot rpm$

Pulley Gear Ratio

$$pulley := \frac{r \cdot 2}{0.875in} = 4.434$$

$$T_{pulley} := \frac{T_{total}}{pulley} = 2.639 \cdot N \cdot m \qquad T_{safe} := T_{pulley} \cdot 1.75 = 4.617 \cdot N \cdot m$$

$S_{pulley} := S_1 \cdot pulley = 133.029 \cdot rpm$

Gearbox:

$ratio := 43 = 43 \quad efficiency := .72$

$$T_{motor} := \frac{\frac{T_{safe}}{ratio}}{efficiency} = 149.142 \cdot 10^{-3} \cdot N \cdot m$$

$$S_{motor} := S_{pulley} \cdot \frac{ratio}{efficiency} = 7944.762 \cdot rpm$$

Given the above specs, chose motor with:

$Motor_T := 170 \cdot 10^{-3} N \cdot m \qquad Motor_S := 7580 rpm$

$T_{motor} := Motor_T \cdot ratio \cdot efficiency = 5.263 \cdot N \cdot m$

$T_{motor} - T_{safe} = 0.646 \cdot N \cdot m$

$$S_{motor} := \frac{Motor_S}{ratio} \cdot efficiency = 126.921 \cdot rpm$$

$S_{motor} - S_{pulley} = -6.108 \cdot rpm$

$T_{motor} > T_{safe} = 1$

$S_{motor} > S_{pulley} = 0$

Shoulder Pivot

$T_{total} := 28.27N \cdot m \qquad \omega_a := \frac{\pi}{2}\frac{rad}{s}$

Spring

$r := 8.4125in = 0.214\,m$

$cir := 2 \cdot 0.3in \cdot \pi = 1.885 \cdot in$

$deflection := 5deg$

$travel := cir \cdot \frac{deflection}{360deg} = 0.026 \cdot in$

$F_{full} := \frac{T_{total}}{r} = 29.743 \cdot lbf \qquad F_{full} = 132.302 \cdot N$

$k := \frac{F_{full}}{2 \cdot travel} = 568.044 \cdot \frac{lbf}{in}$

$\frac{k}{2} = 284.022 \cdot \frac{lbf}{in}$

$def_{max} := 15deg$

$travel_{max} := cir \cdot \frac{def_{max}}{360deg} = 0.079 \cdot in$

$F_{max} := travel_{max} \cdot k = 44.614 \cdot lbf$

$travel_{total} := travel_{max} \cdot 2 = 0.157 \cdot in$

Motor

Desired Specs:

$T_{total} = 28.27 \cdot N \cdot m$

$S_1 := \omega_a = 15 \cdot rpm$

Pulley Gear Ratio

$$pulley := \frac{r \cdot 2}{0.875in} = 19.229$$

$$T_{pulley} := \frac{T_{total}}{pulley} = 1.47 \cdot N \cdot m \qquad T_{safe} := T_{pulley} \cdot 1.75 = 2.573 \cdot N \cdot m$$

$S_{pulley} := S_1 \cdot pulley = 288.429 \cdot rpm$

Gearbox: gearbox: 32mm 8 Nm 320297

$ratio := 21 \qquad efficiency := .83$

$$T_{motor} := \frac{\frac{T_{safe}}{ratio}}{efficiency} = 147.611 \cdot 10^{-3} \cdot N \cdot m$$

$$S_{motor} := S_{pulley} \cdot \frac{ratio}{efficiency} = 7297.59 \cdot rpm$$

Given the above specs, chose motor with:

$Motor_T := 170 \cdot 10^{-3} N \cdot m \qquad Motor_S := 7580 rpm$

$T_{motor} := Motor_T \cdot ratio \cdot efficiency = 2.963 \cdot N \cdot m$

$T_{motor} - T_{safe} = 0.39 \cdot N \cdot m$

$$S_{motor} := \frac{Motor_S}{ratio} \cdot efficiency = 299.59 \cdot rpm$$

$S_{motor} - S_{pulley} = 11.162 \cdot rpm$

$T_{motor} > T_{safe} = 1$

$S_{motor} > S_{pulley} = 1$

Shoulder Rotate

$T_{total} := 2.6N \cdot m$

Spring

$r := \frac{1}{2} in$

$cir := 2 \frac{1.9375}{2} in \cdot \pi = 6.087 \cdot in$

$deflection := 5deg$

$travel := cir \cdot \frac{deflection}{360deg} = 0.085 \cdot in$

$F_{full} := \frac{T_{total}}{r} = 204.724\,N \qquad F_{full} = 46.024 \cdot lbf$

$k := \frac{F_{full}}{2 \cdot travel} = 272.204 \cdot \frac{lbf}{in}$

$\frac{k}{2} = 136.102 \cdot \frac{lbf}{in}$

$def_{max} := 15deg$

$travel_{max} := cir \cdot \frac{def_{max}}{360deg} = 0.254 \cdot in$

$F_{max} := travel_{max} \cdot k = 69.036 \cdot lbf$

$travel_{total} := travel_{max} \cdot 2 = 0.507 \cdot in$

Motor

Desired Specs:

$T_{total} = 2.6 \cdot N \cdot m$

$S_1 := \omega_a = 15 \cdot rpm$

Pulley Gear Ratio

$pulley := \frac{r \cdot 2}{.75in} = 1.333$

$T_{pulley} := \frac{T_{total}}{pulley} = 1.95 \cdot N \cdot m$

$T_{safe} := T_{pulley} \cdot 1.75 = 3.413 \cdot N \cdot m$

$S_{pulley} := S_1 \cdot pulley = 20 \cdot rpm$

Gearbox:

$ratio := 111 \qquad efficiency := .70$

$T_{motor} := \frac{\frac{T_{safe}}{ratio}}{efficiency} = 43.919 \cdot 10^{-3} \cdot N \cdot m$

$S_{motor} := S_{pulley} \cdot \frac{ratio}{efficiency} = 3171.429 \cdot rpm$

Given the above specs, chose motor with:

$Motor_T := 59.9 \cdot 10^{-3} N \cdot m \quad Motor_S := 9340 rpm$

$T_{motor} := Motor_T \cdot ratio \cdot efficiency = 4.654 \cdot N \cdot m$

$T_{motor} - T_{safe} = 1.242 \cdot N \cdot m$

$S_{motor} := \frac{Motor_S}{ratio} \cdot efficiency = 58.901 \cdot rpm$

$S_{motor} - S_1 = 43.901 \cdot rpm$

$T_{motor} > T_{safe} = 1$

$S_{motor} > S_1 = 1$

Appendix E: Joint Lever Arm Calculations

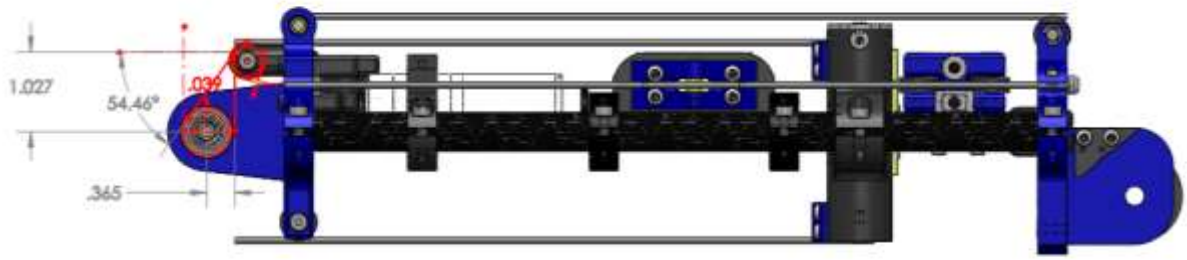

Shoulder Pivot Joint Torque:

Test 1: Elbow bent back, no load

$\tau_m := 4.65N \cdot m$ measured motor torque

$r_m := \frac{0.875}{2}in = 0.438in$ radius of motor pulley

$m_1 := 1.58806kg$ mass of arm

$y_1 := 179.31mm$ horizontal location of center of mass

$\tau_1 := m_1 \cdot y_1 \cdot g = 2.792N \cdot m$ joint torque generate by gravity

$\alpha := 54.46deg$ angle cable contacts pulley

$d_1 := \cos(\alpha) \cdot 1.027in = 0.597in$ lever arm in one direction

$d_2 := \sin(\alpha) \cdot .365in = 0.297in$ lever arm in other direction

$l_1 := d_1 - d_2 = 0.3in$ effective lever arm

$f_m := \frac{\tau_m}{\frac{0.875}{2}in} = 418.448N$ force generated by the motor (cable tension)

$\tau_a := \tau_m \cdot \frac{l_1}{r_m} = 3.188N \cdot m$ torque generated by motor on arm

$efficiency := \frac{\tau_1}{\tau_a} = 0.876$ efficiency

Test 2: Elbow extended, wrist rotate spring box removed

$\tau_m := 5.7N \cdot m$ measured motor torque

$r_m := \frac{0.875}{2} in = 0.438\,in$ radius of motor pulley

$m_2 := 1.48279kg$ mass of arm

$y_2 := 234.81mm$ horizontal location of center of mass

$\tau_2 := m_2 \cdot y_2 \cdot g = 3.414\,N \cdot m$ joint torque generate by gravity

$\alpha := 54.46deg$ angle cable contacts pulley

$d_1 := \cos(\alpha) \cdot 1.027in = 0.597\,in$ lever arm in one direction

$d_2 := \sin(\alpha) \cdot .365in = 0.297\,in$ lever arm in other direction

$l_1 := d_1 - d_2 = 0.3\,in$ effective lever arm

$\tau_a := \tau_m \cdot \frac{l_1}{r_m} = 3.908\,N \cdot m$ torque generated by the motor on the arm

$efficiency := \frac{\tau_2}{\tau_a} = 0.874$ efficiency

Elbow Pivot Tests

Test 3: no load

$\tau_m := 0.9N \cdot m$ measured motor torque

$r_m := \frac{0.875}{2}in = 0.438in$ radius of motor pulley

$m_3 := 0.602kg$ mass of arm

$y_3 := 82.53mm$ horizontal location of center of mass

$\tau_3 := m_3 \cdot y_3 \cdot g = 0.487N \cdot m$ joint torque generate by gravity

$\alpha := 52.83deg$ angle cable contacts pulley

$d_1 := \cos(\alpha) \cdot 2.331in = 1.408in$ lever arm in one direction

$d_2 := \sin(\alpha) \cdot 1.062in = 0.846in$ lever arm in other direction

$l_1 := d_1 - d_2 = 0.562in$ effective lever arm

$\tau_a := \tau_m \cdot \frac{l_1}{r_m} = 0.555N \cdot m$ torque generated by the motor on the arm

$efficiency := \frac{\tau_3}{\tau_a} = 0.877$ efficiency

Test 4: 2.5 lb load

$\tau_m := 4.6N \cdot m$ measured motor torque

$r_m := \frac{0.875}{2}in = 0.438in$ radius of motor pulley

$m_4 := 1.75kg$ mass of arm

$y_4 := 156.38mm$ horizontal location of center of mass

$\tau_4 := m_4 \cdot y_4 \cdot g = 2.684N \cdot m$ joint torque generate by gravity

$\alpha := 52.83deg$ angle cable contacts pulley

$d_1 := \cos(\alpha) \cdot 2.331in = 1.408in$ lever arm in one direction

$d_2 := \sin(\alpha) \cdot 1.062in = 0.846in$ lever arm in other direction

$l_1 := d_1 - d_2 = 0.562in$ effective lever arm

$\tau_a := \tau_m \cdot \frac{l_1}{r_m} = 2.839N \cdot m$ torque generated by the motor on the arm

$efficiency := \frac{\tau_4}{\tau_a} = 0.945$ efficiency

Test 5: 3 lb load

$\tau_m := 5.4N \cdot m$ measured motor torque

$r_m := \frac{0.875}{2}in = 0.438in$ radius of motor pulley

$m_5 := 1.977kg$ mass of arm

$y_5 := 161mm$ horizontal location of center of mass

$\tau_5 := m_5 \cdot y_5 \cdot g = 3.121N \cdot m$ joint torque generate by gravity

$\alpha := 52.83deg$ angle cable contacts pulley

$d_1 := \cos(\alpha) \cdot 2.331in = 1.408in$ lever arm in one direction

$d_2 := \sin(\alpha) \cdot 1.062in = 0.846in$ lever arm in other direction

$l_1 := d_1 - d_2 = 0.562in$ effective lever arm

$\tau_a := \tau_m \cdot \frac{l_1}{r_m} = 3.333N \cdot m$ torque generated by the motor on the arm

$efficiency := \frac{\tau_5}{\tau_a} = 0.937$ efficiency